NEW PHYSICAL FOUNDATIONS FOR REMOTE SENSING ESTIMATION

OF LIVE FUEL MOISTURE CONTENT AND FIRE DANGER

by

Yi Qi

A dissertation submitted to the faculty of
The University of Utah
in partial fulfillment of the requirements for the degree of

Doctor of Philosophy

Department of Geography

The University of Utah

December 2014

The University of Utah Graduate School

STATEMENT OF DISSERTATION APPROVAL

The dissertation of **Yi Qi**

has been approved by the following supervisory committee members:

Philip E. Dennison	, Chair	**May 12, 2014** Date Approved
Richard R. Forster	, Member	**May 12, 2014** Date Approved
Simon Brewer	, Member	**May 12, 2014** Date Approved
David Bowling	, Member	**May 12, 2014** Date Approved
William Matt Jolly	, Member	**June, 11, 2014** Date Approved

and by **Andrea Brunelle** , Chair of

the Department of **Geography**

and by David B. Kieda, Dean of The Graduate School.

ABSTRACT

Wildfire is a multifaceted, global phenomenon with ecological, environmental, climatic and socioeconomic impacts. Live fuel moisture content (LFMC) is a critical fuel property for determining fire danger. Previous research has used meteorological data and remote sensing to estimate LFMC with the goal of extending direct ground measurement. A fundemental understanding of plant physiology and spectral response to LFMC variation is needed to advance use of LFMC for fire risk management and remote sensing applications. This study integrates field samples of three species, lab measurements, remote sensing data and statistical analysis to construct a more complete knowledge of the physical foundations of LFMC seasonality from three perspectives: 1) relationships between soil moisture and LFMC; 2) spectroscopic analysis of seasonal changes in LFMC and leaf dry mass; 3) relationships between LFMC and leaf net heat content, and between leaf net heat content and remotely sensed indices. This study is the first to demonstrate a relationship between *in situ* soil moisture and LFMC. It also challenges the current asumption of changing water content and stable dry matter content over time in remote sensing esimation of LFMC, showing the dominant contribution of dry matter in LFMC variation in some conifer species. The results demonstrate the combination of spectroscopic data and partial least squares regression can improve modeling accuray for LFMC temporal variation, but the spectral response to changing LFMC and dry mass is difficult to seperate from broader spectral trends due to temporal

change in chlorophyll, leaf structure, water and covaried biochemical components. Lastly it introduces a new vegetation variable, leaf net heat content, and demostrates its relationship with LFMC and potential for remote sensing estimation. This study will improve present capabilities of remote sensing for monitoring vegetation water stress and physiological properties. It will also advance understanding of seasonal changes in LFMC to better estimate fire danger and potential impacts of fire on ecosystems and the carbon cycle.

TABLE OF CONTENTS

LIST OF FIGURES

LIST OF TABLES

ACKNOWLEDGMENTS

First and foremost, I sincerely appreciate my advisor, Dr. Philip Dennison, for his strong mentorship in my graduate student years. Thank you Phil, for believing in me and bringing me to the lab! From the beginning Phil has been consistently supporting me in every aspect of research and life. Phil always encourages me to pursue my research interests and questions, guides me through research, leads me to many great opportunities, provides all-possible resources, consults with me on professional and personal hurdles, revises manuscripts with tremendous patience, and most importantly, sets up a role model for me both academically and personally. I feel very fortunate to have Phil as my advisor, and I heartily look forward to maintaining the close bond and collaborations.

I also have great appreciation to my committee members. Dr. Matt Jolly kindly hosted me in the summer of 2012 in Missoula and provided guidance for field work and lab experiments. Dr. Dave Bowling led me to learn a lot about plant ecology and physiology. Dr. Simon Brewer sharpened my understanding about statistical modeling. Dr. Rick Forster taught me in two remote sensing classes. Their wisdom and guidance helped me to move the study forward. A special thank you must go to my collaborator, Rachael Kropp, who helped me on every field trip and collected a tremendous amount of data. Without her hard work I would not be able to finish the dissertation. I am indebted to the help from many faculties, classmates and friends. The URSA Lab provided a friendly teamwork environment and group discussion on many interesting topics.

CHAPTER 1

INTRODUCTION

Wildfire is a significant disturbance in the terrestrial biosphere. It results in significant CO_2 emission which contributes to climate change, carbon sink-source conversion and ecosystem function transition (Bowman et al. 2009; Cochrane 2003; Van Der Werf et al. 2006). It is a devastating hazard which causes considerable fatalities and economic loss and escalates the cost of fire suppression and damage mitigation (FAO 2001). The severity and impact of fires in the United States have increased over the past two decades, with higher large-wildfire frequency and longer fire seasons in western US forests (Westerling et al. 2006). These are correlated with higher spring and summer temperatures and earlier snowmelt (Running 2006). Increased temperature in the future will likely extend fire seasons throughout the western US, with more fires occurring earlier and later than is currently typical, and will increase the total area burned in some regions (McKenzie et al. 2004). If climatic change increases the amplitude and duration of extreme fire weather, we can expect significant changes in the distribution and abundance of dominant plant species in some ecosystems. This would thus affect habitat for sensitive plant and animal species. Thus it is important to develop scientific methods to estimate wildfire danger for fire management and risk mitigation.

Live fuel moisture content (LFMC) is defined as the ratio of water content to dry

matter content in live vegetation. LFMC is an important fuel property controlling both fire ignition probability and fire spread rates (Rothermel 1972). The direct measurement of LFMC is done by collecting fresh field samples, drying them until all moisture is evaporated, and calculating the water content using the mass difference between fresh and dry samples (Lawson and Hawkes 1989; Pollet and Brown 2007). Field sampled LFMC represents conditions for a vegetation type at a single site and time, and it is difficult to extrapolate field measurements to larger regions and longer time periods.

Seasonal LFMC change is fundamentally controlled by soil water availability and plant physiological processes. Previous studies have used meteorological data, such as precipitation and temperature, as water-stress indicators to estimate LFMC (e.g., Dennison et al. 2003; Dennison and Moritz 2009). The second chapter seeks to examine the empirical relationship between soil moisture and LFMC by field sampling two species in Northern Utah, Gambel oak (*Quercus gambelii* Nutt) and big sagebrush (*Artemisia tridentata* Nutt). This is the first analysis comparing *in situ* soil moisture measurements and field-collected LFMC.

Both water and dry matter change during the plant phenological cycle, resulting in seasonal LFMC variation. Vegetation reflectance spectra change in response to variation in plant physiological status, such as the foliar concentration of water, dry matter, pigment, and leaf structure. Remote sensing data offer a potentially cost-effective way to improve LFMC temporal and spatial monitoring. Previous studies have used various empirical methods and physical-based radiative transfer modeling methods to estimate LFMC. Common assumptions in early works were stable dry matter and varied water content over time. However, physiological studies have shown that dry matter changes

over the growth season and dominates LFMC change in comparison to water content (e.g., Kozlowski and Clausen 1965; Jolly et al. 2014). In the third chapter I conduct a temporal monitoring of plant LFMC and spectroscopic data of two species, lodgepole pine (*Pinus contorta* Douglas ex Loudon) and big sagebrush (*Artemisia tridentata* Nutt). This study provides a more complete understanding of: 1) how water and dry matter contribute to LFMC variation over time; 2) how spectroscopic data respond to water and dry matter change over time.

As a ratio of water to dry matter, LFMC has been used as an indirect indicator of fire danger. Heat content (energy produced by combustion of dry matter) is an additional variable related to fire danger. Semi-empirical fire behavior models (e.g., Rothermel 1972) assume constant dry matter over time and across species. The findings in the third chapter challenged this assumption. Decreasing water or increasing dry matter may result in similar LFMC "dry-down" trends, but the potential fire danger and energy release would be significantly different. The fourth chapter introduces a new variable, leaf net heat content (LNHC), to capture both water and dry matter contribution to net energy produced by combustion, serving as a complementary metric to LFMC. This chapter also tests the possibility of using remote sensing to estimate LNHC as leaf and canopy scale.

In total, this dissertation investigated the physical foundation of LFMC from three perspectives. It intended to explain the nature of LFMC variation and to inform new insights for the remote sensing applications of LFMC.

CHAPTER 2

SOIL MOISTURE AND LIVE MOISTURE CONTENT

2.1 Introduction

Live fuel moisture content (LFMC) is an important fuel property for assessing fire danger. LFMC is defined as the proportion of water content to dry matter content in live vegetation. LFMC has been incorporated in fire danger rating systems, such as the National Fire Danger Rating System (NFDRS) in the US (Deeming et al. 1978) and the Canadian Forest Fire Danger Rating System (CFFDRS) (Stocks et al. 1989). LFMC can also be used by fire behavior models to determine energy needed for ignition and fire spread rate (Rothermel 1972). The direct measurement of LFMC is done by collecting fresh field samples, drying them until all moisture is evaporated, and calculating the water content using the mass difference between fresh and dry samples (Lawson and Hawkes 1989; Pollet and Brown 2007). Field sampled LFMC represents conditions for a vegetation species at a single site and time, and it is difficult to extrapolate field measurements to larger regions and longer time periods.

Previous studies have used meteorological indices to estimate LFMC (Burgan et al. 1998; Sebastián-López et al. 2002; Viegas et al. 2001). Although weather data are easily accessible, two problems still challenge meteorological indices: first, meteorological indices assume a constant relationship between observed parameters and

LFMC; and second, meteorological data are still linked to point observations that may not be representative of larger areas. LFMC is fundamentally controlled by the plant physiological processes and soil water availability, so meteorological indices may not reflect local variation in topography, soil type, precipitation, and vegetation type and cover. Weather conditions like foehn winds can also complicate relationships between meteorological data and LFMC.

Remote sensing data have been proposed for use in LFMC estimation to improve spatial and temporal coverage. Most empirical studies have used band-ratio indices or radiative transfer models (RTM) to correlate variables based on vegetation greenness or moisture content with field-measured LFMC. Results of previous studies have varied across study sites and species (Dennison et al. 2005; Roberts et al. 2006; Yebra et al. 2008). Another potential proxy for LFMC, soil moisture, has not previously been compared to field-measured LFMC. My research investigates four potential proxies for LFMC that could improve spatial and/or temporal coverage of LFMC estimation. Soil moisture responds to precipitation and evapotranspiration, and soil moisture measurements can be done continuously. Remote sensing provides extensive spatial coverage with a temporal resolution similar to current LFMC sampling protocols (Dennison et al. 2005). The objectives of this research are to: 1) examine relationships between soil moisture and LFMC and determine whether soil moisture has potential as an LFMC proxy, and 2) compare soil moisture to more established remote sensing indices as proxies for LFMC estimation.

2.2 Background

Seasonal LFMC variation is controlled by precipitation, soil moisture, evapotranspiration, and plant physiological processes. Water is transported along a water potential gradient in the soil-plant-atmosphere continuum. The soil water potential generally declines with decreasing soil moisture, and corresponding plant water uptake drops due to smaller hydraulic conductance between soil and root (Schulze et al. 2005). Soil moisture available to vegetation is controlled by soil properties, precipitation and evapotranspiration fluxes over time scales of weeks to years. In extreme conditions rapid decrease in LFMC can happen in days, for example, during Santa Ana winds affecting southern California. The relationship between drought and fuel moisture is presumably that low precipitation and/or high evapotranspiration result in lower LFMC and increase wildfire area burned (Bessie and Johnson 1995; Chuvieco et al. 2009; Keetch and Byram 1968; Littell et al. 2009).

LFMC trends in southern California chaparral have been predicted using seasonal precipitation (Dennison et al. 2008) and monthly precipitation terms (Dennison and Moritz 2009). Previous studies have designed soil water indices to estimate LFMC. Dimitrakopoulos and Bemmerzouk (2003) demonstrated a strong relationship between Keetch Byram Drought Index (KBDI) (Keetch and Byram 1968) and LFMC for herbaceous understory vegetation in a Mediterranean pine forest. KBDI uses precipitation and maximum temperature to estimate the net effect of daily precipitation and evapotranspiration on soil water balance. Dennison et al. (2003) found a strong, nonlinear relationship between a cumulative water balance index (CWBI) model and LFMC in chaparral. CWBI cumulatively sums precipitation and reference evapotranspiration over

time. More complex than the standard KBDI, the Dennison et al. (2003) CWBI calculated reference evapotranspiration from a modified Penman equation (Snyder and Pruitt 1992) using solar irradiance, air temperature, vapor pressure and wind speed, but did not take into account plant physiological processes. No previous study has directly compared *in situ* soil moisture measures to field-sampled LFMC.

Remote sensing offers a potentially cost-effective way to improve LFMC temporal and spatial monitoring. The reflectance spectrum of vegetation contains absorption features that result from harmonics and overtones of various foliar chemical components (Curran 1989). At the leaf level, the typical spectral features of green vegetation include chlorophyll absorption in the visible (400-700 nm), leaf structure expressed in the near infrared (NIR, 700-1300 nm) and water absorption dominating in the shortwave infrared (SWIR, 1300-2500 nm) (Bowyer and Danson 2004; Ceccato et al. 2001). At the canopy level, reflectance is a function of solar and view geometry, leaf-level reflectance, canopy structure, and vegetation cover. As LFMC declines, visible and SWIR reflectance generally increase while NIR reflectance decreases (Figure 2.1). Changes in NIR reflectance and water absorption with changing LFMC can be used to predict LFMC from remote sensing data (Chuvieco et al. 2002; Dennison et al. 2005). Changes in indices measuring chlorophyll absorption have also been correlated with changes in LFMC (Roberts et al. 2006; Stow et al. 2006), since vegetation greenness measures have shown good correlation with moisture content in ecosystems such as grasslands and shrublands.

Remote sensing data have been proven useful for estimating LFMC using empirical methods and radiative transfer models (RTM) (Chuvieco et al. 2009). Most
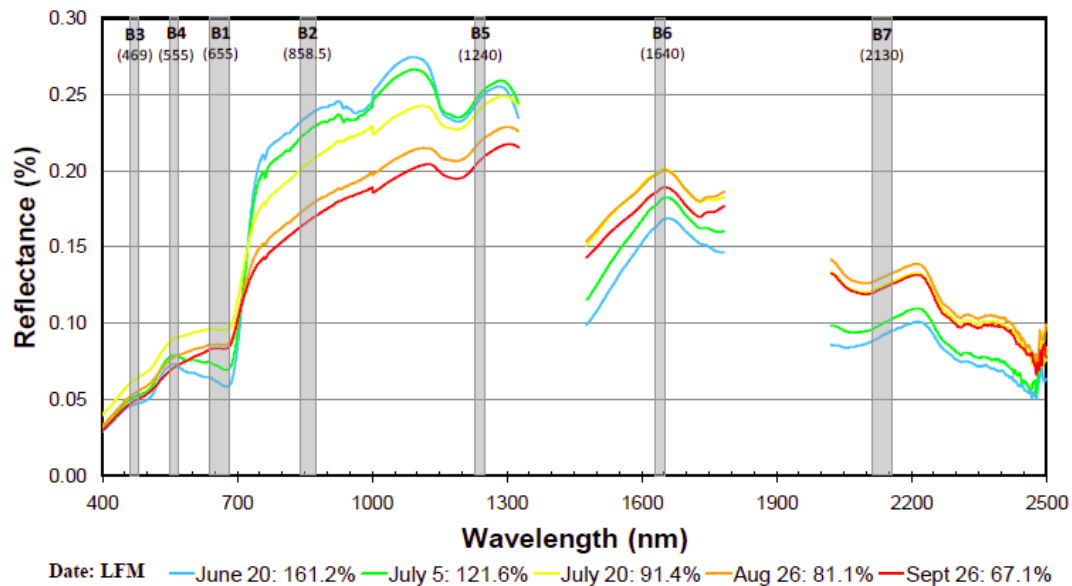
Figure 2.1 An example of field reflectance spectra (400-2500nm) for sagebrush collected over the summer of 2005. As the line colors change from blue to red, LFMC decreases. MODIS bands (grey) with their central wavelength (in parentheses) are also shown.

empirical studies have used regression analyses to compare vegetation indices with field-measured LFMC (e.g., Dennison et al. 2005; Roberts et al. 2006; Stow et al. 2006). RTM simulates the reflection, absorption, and transmission of electromagnetic radiation at leaf and canopy scales and has been mathematically inverted to estimate canopy water content and LFMC (Riaño et al. 2005; Trombetti et al. 2008; Yebra and Chuvieco 2009; Zarco-Tejada 2003). Many previous papers have focused on Mediterranean vegetation, such as chaparral in southern California (Dennison et al. 2005; Roberts et al. 2006; Serrano et al. 2000; Ustin et al. 1998), and herbaceous vegetation and shrubland in Spain (Chuvieco et al. 2003, 2004). Yebra et al. (2008) found that empirical and RTM methods had comparable performance for LFMC estimation in Mediterranean vegetation, but RTM was more robust for applications across different species and sites.

2.3 Methods

I conducted this research at ten sites in northern Utah, USA (Table 2.1). Two species, Gambel oak (*Quercus gambelii* Nutt) and big sagebrush (*Artemisia tridentata* Nutt) were studied at five sites each (Table 2.1). These sites were chosen because they were operational LFMC field sampling sites for the US Bureau of Land Management (BLM) or Forest Service (USFS). The sites were within a geographic region approximately 8800 km^2 in size, and cover large gradients in elevation (1582 – 2073 m), slope (2 – 33 degrees), vegetation cover and meteorological conditions.

Field sampled LFMC data were downloaded from the National Fuel Moisture Database (NFMD: http://www.wfas.net/index.php/national-fuel-moisture-database-moisture-drought-103, last accessed in May 2014). Standard protocols for LFMC sampling established by Pollet and Brown (2007) were followed by BLM and USFS personnel. Live foliage and pliable small stem material (up to 0.32 cm [1/8 in] diameter) were clipped from Gambel oak and sagebrush shrubs. Several shrubs were sampled at different height and aspects. Samples were stored in containers with tight-fitting lids and kept cool and dry. The samples were weighed in the field to provide wet mass, and then were dried in a mechanical convection oven for at least 24 hours at 100 ^{o}C and reweighed to provide dry mass. LFMC was calculated by dividing the water mass (wet mass – dry mass) by dry mass. LFMC was generally sampled biweekly during the summer and fall without regard for leaf age, and species names, sampling dates; LFMC values were submitted to the NFMD.

In the summer of 2009 and 2010, soil moisture stations were installed at LFMC sampling locations in collaboration with BLM and USFS personnel. At each site, a 15 cm

Table 2.1 Description of ten study sites in northern Utah, USA including geographic locations, species, soil texture at 20cm depth, slope (degrees), aspect (in degrees from north), elevation (meters), soil moisture measurement start date, number of LFMC observations, and maximum and minimum of LFMC measurements (%).

Site	Latitude	Longitude	Species	Soil Texture	Slope	Aspect	Elevation	Start Date	N	Max LFMC	Min LFMC
Little Cottonwood	40.57	-111.77	Gambel oak	Loamy sand	15	208	1718	5/18/09	26	191	79
Hobble Creek	40.15	-111.54	Gambel oak	Sandy loam	33	202	1910	6/6/10	14	217	76
Maple Canyon	40.13	-111.53	Gambel oak	Sandy loam	29	162	1870	6/6/10	16	201	79
Squaw Peak	40.30	-111.62	Gambel oak	Clay	8	50	2073	6/8/10	12	152	81
Black Cedar	38.98	-112.24	Gambel oak	Clay loam	6	285	1979	6/7/10	20	231	89
Vernon	40.06	-112.33	big sagebrush	Gravelly loam	2	35	1712	4/28/09	59	237	57
Mud Springs	39.88	-112.22	big sagebrush	Sandy loam	6	18	1790	5/5/09	38	221	67
Muskrat	40.64	-112.65	big sagebrush	Very gravelly loam	16	259	1582	6/3/10	36	210	63
Sevier Reservoir	39.33	-112.06	big sagebrush	Sandy loam	9	44	1662	6/7/10	22	197	71
Black Cedar	38.98	-112.24	big sagebrush	Clay	6	285	1979	6/7/10	22	230	78

(6 in) diameter hole was dug and four Decagon 5TE probes were inserted into the hole wall. Rocky soils prevented deep probe placement at many of the sites, so probes were placed at all sites as follows: two at a depth of 20 cm, and two at 40 cm. Volumetric soil water content (m^3 m^{-3}) and soil temperature (^{o}C) were recorded by a Decagon Em50 data logger every 60 min. Measurements over 24 hour periods were averaged to provide daily soil moisture values. Since incomplete contact with the soil can result in low measured soil moisture, the probe with the highest average moisture at 20 cm depth was used for further analysis. Incomplete data were available for the Black Cedar Gambel oak site after the data logger was accidentally disconnected from the probes, likely due to disturbance by grazing cattle.

The Terra Moderate Resolution Imaging Spectroradiometer (MODIS) surface reflectance product MOD09A1 was used to calculate remote sensing measures. MOD09A1 is an 8-day composite product of atmospherically corrected reflectance for the first seven spectral bands of the MODIS instrument at 500 m spatial resolution (bands shown in Figure 2.1). The original products were downloaded from the Oak Ridge National Laboratory MODIS Global Subsets site (http://daac.ornl.gov/cgi-bin/MODIS/GLBVIZ_1_Glb/modis_subset_order_global_col5.pl, last accessed in May 2014). Cloud and bad band data were masked using a MODIS quality assurance layer. The 500 m pixel containing each soil moisture/LFMC sampling site was extracted and three remote-sensing based measures were calculated from MODIS bands: normalized difference vegetation index (NDVI), normalized difference water index (NDWI) and canopy water content (CWC). NDVI is a normalized ratio between NIR and red reflectance (Rouse et al. 1973) that captures both chlorophyll absorption in the visible

and leaf additive reflectance in the NIR spectral region:

$$\frac{\rho_{856} - \rho_{655}}{\rho_{856} + \rho_{655}}$$

where the subscript indicates the band center wavelength in nm. Higher NDVI values indicate higher chlorophyll absorption, leaf area and vegetation cover. NDWI is a normalized ratio between a NIR band and a SWIR band that can be used for estimating vegetation liquid water content (Gao 1996):

$$\frac{\rho_{856} - \rho_{1240}}{\rho_{856} + \rho_{1240}}$$

NDVI and NDWI have shown strong correlations with LFMC in previous studies (Roberts et al. 2006; Stow et al. 2006). CWC was calculated by an inversion of a radiative transfer model through an artificial neural network (ANN) (Trombetti et al. 2008) combined with NDVI and normalized difference indices using 1640 nm and 2130 nm as absorption bands. The Prospect-SailH radiative transfer model (Jacquemoud et al. 1995; Kuusk 1995) was used by Trombetti et al. (2008) to derive CWC. The CWC (expressed in mm) was computed as the product of leaf area index and leaf water content, which was defined as the theoretical thickness of a single layer of water per unit leaf area. Modeled CWC is not equivalent to LFMC, since LFMC is dependent on the amount of dry matter in relation to CWC. However, if dry matter remains relatively stable over time, then CWC and LFMC should be strongly correlated.

For each site I conducted regression analyses between LFMC and each independent variable, including soil moisture, CWC, NDVI and NDWI. Coefficient of determination (R^2) of the four bivariate linear regression models were calculated to investigate performance of soil moisture and remote sensing proxies in explaining LFMC

variation. I calculated the mean absolute error (MAE) for each regression model to measure the average magnitude of LFMC estimation errors. To test the model performance across sites and species, I applied regression models to pooled datasets among and between species. LFMC variation is dependent on local characteristics of individual sites. To eliminate cross-site diversity within the pooled data, an offset was calculated for each proxy as its value subtracted by its mean value for that site, then these offsets were pooled together from all sites. Bootstrap validation was employed to test the robustness of each model for the pooled data. For each explanatory parameter, a random number of observations were taken out with replacement from the samples, and a new linear regression model was constructed. I then calculated the R^2, calibration error (root mean square error of residuals between predicted and observed LFMC of all observations) and validation error (root mean square error of residuals between predicted and observed LFMC of taken-out observations) of the new model. The bootstrap validation was repeated 1000 times to examine the model robustness.

2.4 Results

Time series of LFMC demonstrated seasonal pattern of green-up in early spring and drying down through late spring and summer. The amplitude and timing of seasonal changes varied considerably between years. An example is provided by the Vernon big sagebrush site (Figure 2.2). Big sagebrush LFMC measurements started at 200 % LFMC at day 110 in 2010 and 154 % LFMC at day 103 in 2011. LFMC peaked and decreased earlier in 2010 than 2011. Both years showed similar LFMC in late summer and a slight increase of LFMC in the fall, but this happened about 15 days earlier in 2011. All proxies
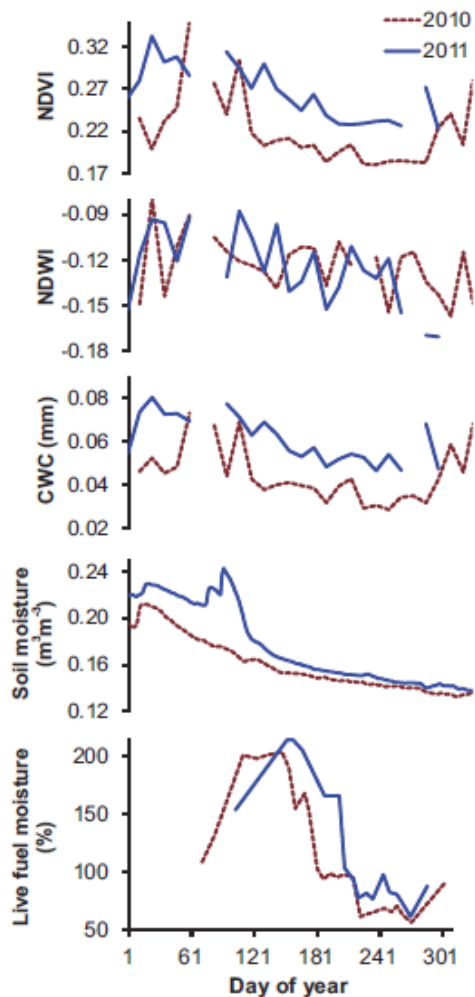
Figure 2.2 2010 and 2011 time series plots for the Vernon big sagebrush site. Some remote sensing measures are missing following removal by quality assessment.

generally decreased at different rates. In 2011, soil moisture spiked due to precipitation events in spring and then gradually declined over the season.

Strength of correlations between LFMC and the four independent variables varied across sites (Table 2.2). Soil moisture showed positive relationships with LFMC and the highest R^2 value (0.66) when averaged across all ten sites. The R^2 values for soil moisture were generally higher than those for remote sensing variables, with the exception of big

Table 2.2 R^2 and mean absolute error (MAE) of bivariate linear regression results between LFMC and soil moisture or remote sensing variables.

Site	CWC		NDVI		NDWI		Soil Moisture	
	R^2	MAE	R^2	MAE	R^2	MAE	R^2	MAE
Little Cottonwood	0.38**	17.66	0.13	21.98	0.22*	21.65	0.63***	14.15
Hobble Creek	0.36*	20.12	0.4*	18.35	0.24	24.13	0.86***	9.76
Maple Canyon	0.12	21.77	0.01	24.36	0.38*	18.09	0.86***	10.72
Squaw Peak	0.7***	8.63	0.58**	9.61	0.69***	9.77	0.89***	5.14
Black Cedar	0.01	26.59	018	25.61	0.06	28.1	0.53***	18.45
Vernon	0.34***	33.49	0.39***	31.81	0.38***	33.98	0.65***	24.51
Mud Springs	0.6***	22.39	0.62***	22.36	0.46***	27.59	0.46***	28.79
Muskrat	0.39***	25.35	0.75***	15.44	0.22**	31.61	0.41***	22.87
Sevier Reservoir	0.45***	20.06	0.46***	19.7	0.24*	26.95	0.63***	19.52
Black Cedar	0.02	34.09	0.01	34.05	0.02	34.05	N/A	N/A
Average of Gambel oak	0.32	18.69	0.26	19.98	0.32	20.35	0.75	11.64
Average of big sagebrush	0.36	27.07	0.44	24.67	0.26	30.84	0.54	23.92
Average of all sites	0.34	22.88	0.35	22.33	0.29	25.59	0.66	17.1
Pooled Gambel oak	0.13***	19.74	0.01	22.29	0.12***	20.97	0.65***	13.31
Pooled big sagebrush	0.31***	31.52	0.26***	32.68	0.24***	34.08	0.48***	20.04
Pooled all sites	0.27***	28.05	0.15***	31.45	0.18***	31.53	0.49***	23.97

N/A: No analysis due to bovine disturbance of soil moisture data logger
Significance level: *** $P< 0.001$, ** $P< 0.01$, * $P< 0.05$

sagebrush sites at Mud Springs and Muskrat. Values of R^2 for soil moisture were also more stable across sites. The weakest relationship for soil moisture was for big sagebrush at the Muskrat site, with an R^2 value of 0.41. The strongest relationship for soil moisture was Gambel oak at the Squaw Peak site, where the R^2 of the relationship with LFMC was 0.89. Mean of MAE across all sites was lowest for soil moisture, with a mean MAE of 17.1 % LFMC. The smallest MAE was 5.14 % at the Squaw Peak Gambel oak site, while the largest MAE was 28.79 % for big sagebrush at Mud Springs. For species averages, Gambel oak showed higher R^2 and smaller MAE than big sagebrush.

Among the remote sensing measures each regression model showed wide variation within sites of same species and between species (Figures 2.3 and 2.4). The highest R^2 values of each variable were found at Squaw Peak with CWC (0.7), Muskrat with NDVI (0.75), and Squaw Peak with NDWI (0.69). All remote sensing measures had smaller averaged R^2 values than soil moisture, and multiple measures had weak correlations with LFMC ($R^2 < 0.2$) at Maple Canyon and Black Cedar. NDVI had stronger correlations than CWC and NDWI at six sites, and NDVI had a slightly higher averaged R^2 of 0.35. Comparing the two species, CWC and NDVI showed stronger correlations with big sagebrush, but NDWI had a higher averaged R^2 with Gambel oak. MAE results also varied across sites and proxies within a range between 8.6 % and 34 % LFMC. Mean MAE values were 22.3 % for NDVI, 22.9 % for CWC, and 25.6 % for NDWI. Soil moisture had smaller MAE values than the remote sensing proxies at all five Gambel oak sites and two big sagebrush sites, except Mud Springs and Muskrat. Gambel oak had smaller averaged MAE values for remote sensing variables than big sagebrush. Some soil moisture values diverged from the general trends, for example, in the big sagebrush sites
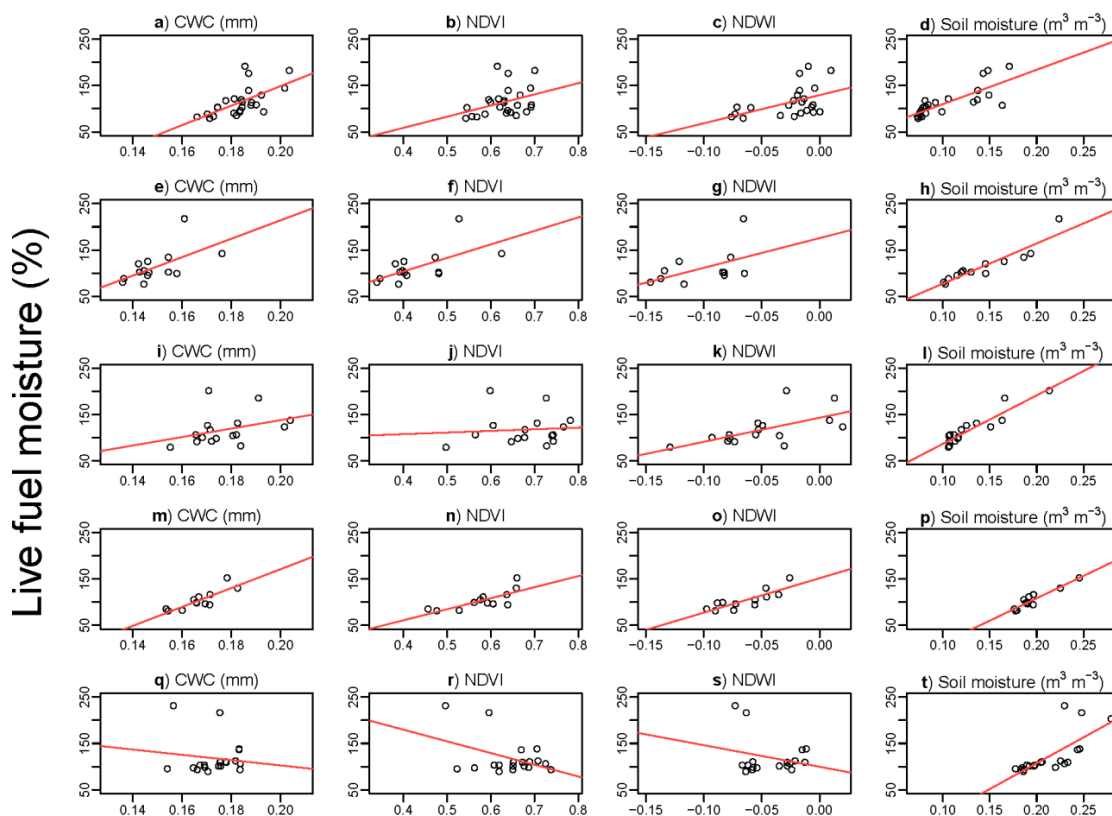
Figure 2.3 Plots of MODIS-derived CWC, NDVI, NDWI and soil moisture against LFMC for Gambel oak sites. (a-d) Little Cottonwood Canyon, (e-h) Hobble Creek, (i-l) Maple Canyon, (m-p) Squaw Peak, (q-t) Black Cedar. The red lines indicate best fit linear equations.

Vernon (Figure 2.4d) and Muskrat (Figure 2.4i). According to the historical weather and soil moisture data, many abnormally high soil moisture values were observed following precipitation events. Soil moisture was higher in the short-term, while LFMC changed more slowly with a peak that lagged peak soil moisture (Figure 2.2).

In the regression models for pooled datasets, soil moisture showed the strongest correlation with a R^2 of 0.65 for Gambel oak, 0.48 for big sagebrush and 0.49 for all sites (Figure 2.5). Across all sites and across individual species, CWC had a higher pooled R^2
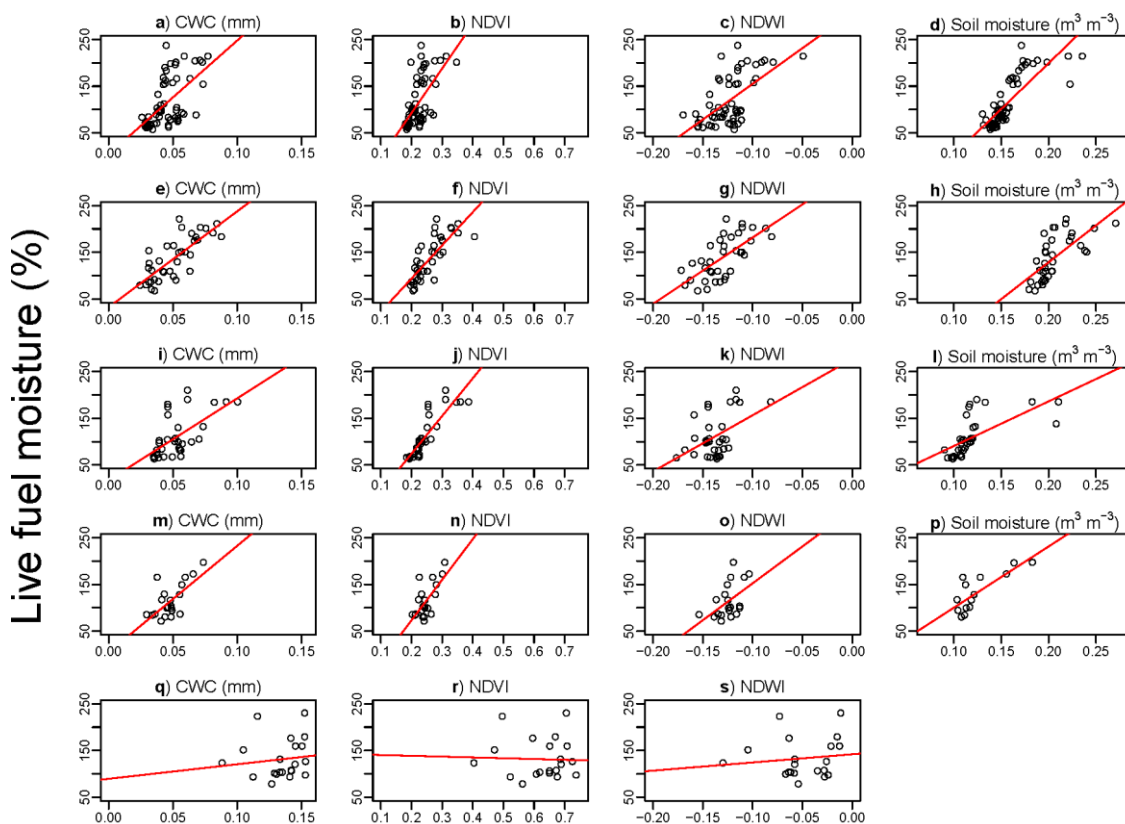
Figure 2.4 Plots of MODIS-derived CWC, NDVI, NDWI and soil moisture against LFMC for big sagebrush sites. (a-d) Vernon, (e-h) Mud Spring, (i-l) Muskrat, (m-p) Sevier Reservoir, (q-s) Black Cedar. The red lines indicate best fit linear equations.

than NDVI and NDWI. For remote sensing measures big sagebrush had higher pooled R^2 values. Soil moisture had smaller MAE than other proxies, and Gambel oak sites had smaller MAE than big sagebrush sites (Table 2.2). Boxplots shown in Figure 2.6 demonstrate the range of R^2 values, calibration errors, and validation errors from bootstrap validation. Soil moisture showed a median R^2 of 0.5 across all sites, followed by CWC, NDWI and NDVI. Soil moisture also had the smallest calibration error and validation error. The stronger correlations with soil moisture were maintained for both
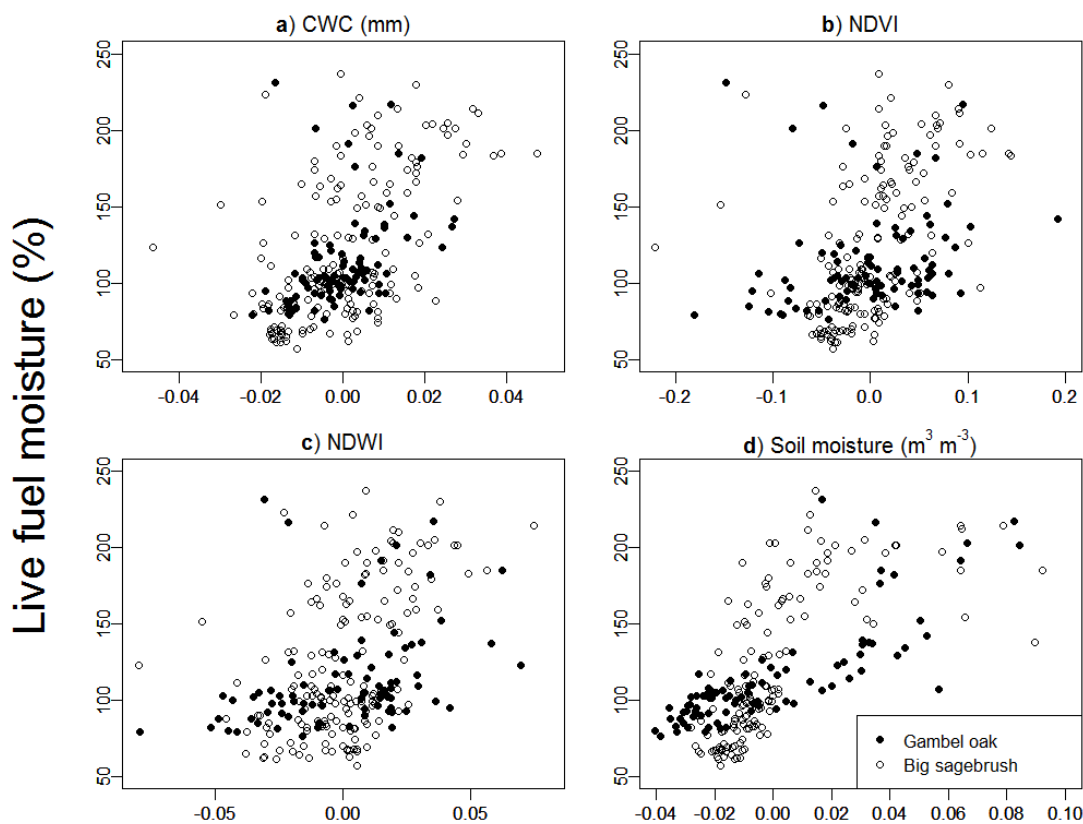
Figure 2.5 Plots of soil moisture and MODIS-derived CWC, NDVI, and NDWI after offset adjustment and pooling for all 10 sites. Black circles correspond to Gambel oak, and open circles correspond to big sagebrush.

species. The three remote sensing proxies had higher R^2 for big sagebrush than Gambel oak. CWC showed consistently better performance than the two indices. NDVI had stronger correlations than NDWI only for big sagebrush. The calibration errors and validation errors for big sagebrush were generally larger than those for Gambel oak.

2.5 Discussion

The regression models and bootstrap validation demonstrated that soil moisture was most strongly correlated with LFMC in both species and across sites. The median R^2
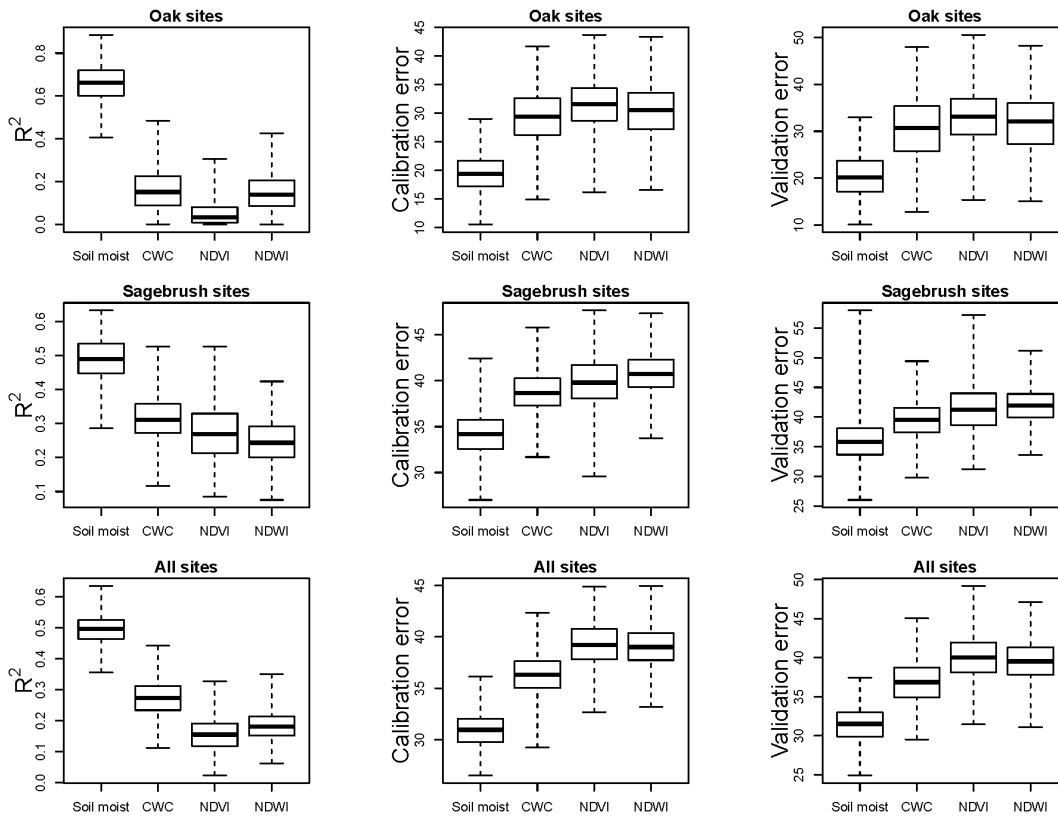
Figure 2.6 Boxplots of bootstrap validation for R^2 (left column), calibration error (middle column), and validation error (right column) for Gambel oak (top row), big sagebrush (middle row) and all sites (bottom row). The bottom and top ends of the whiskers represent the minimum and maximum. The bottom and top of the box represent the first and third quartiles. The band near the middle of the box represents the median.

of validation showed that about 50 % LFMC variation was explained by soil moisture in the pooled data. The unexplained variation might be partially related to soil depth, soil available water capacity, and plant physiological processes. The soil available water capacity, the water content between field capacity and wilting point, is determined by soil texture. Some Gambel oak sites had fine soil texture, like clay loam at Black Cedar and clay at Squaw Peak. However, big sagebrush sites had coarse soil texture including sandy loam and gravelly loam (Table 2.1). Fine soil with narrow pore spacing can hold more water than coarse soils with wide pore spacing. Given the same meteorological

conditions, soil at Gambel oak sites might provide more available water to support plants than soil at big sagebrush sites. I did not have soil depth data for my sites. The minimum root depth of big sagebrush is 40 cm, and Gambel oak is 90 cm with site-dependent variation (USDA Plants Database: http://plants.usda.gov/java/, last accessed in May 2014). Both species have a deep taproot coupled with laterally diffused roots near the surface, allowing plants to absorb water from both surface precipitation and the water table several meters beneath. In addition, soil moisture may increase rapidly due to precipitation recharge, while LFMC exhibits a lagged response. The spatial variability of soil moisture can be influenced by small scale factors such as soil type, topography and vegetation species, and large scale factors such as variability in precipitation and evapo-transpiration (Brocca et al. 2007; Entin et al. 2000). A single soil moisture station at each site cannot capture local spatial variation in soil moisture. Some of my sites were on steeper slopes, where the local hydraulic drainage conditions were different from flat sites. This might partially cause the wide variation of R^2 values among sites. In addition, big sagebrush hydraulically redistributes water from deeper depths to shallower depths and has high tolerance to drought and restricted water conditions (Kolb and Sperry 1999; Richards and Caldwell 1987). Thus sagebrush may be less vulnerable to soil moisture variation than Gambel oak. At larger scales, my ten sites covered a geographical region in northern Utah with varied topography, ecosystem and weather conditions. As a result, pooling data across multiple years and sites incorporated different seasonality and interannual variation into the regression models, which partially contributed to small R^2 and large MAE for some sites and pooled data across species.

Among the three remote sensing proxies, CWC showed the best regression results

with higher R^2 in the pooled data and smaller validation errors. This demonstrates the comparative advantages of using RTM across sites and species rather than relying on band-ratio indices. Between the two indices, NDVI showed slightly better explanatory performance than NDWI for big sagebrush sites and pooled data, but NDVI had weak correlation with LFMC for Gambel oak sites. There are several potential factors that could influence the strength of correlations between LFMC and remote sensing measurements. Although MODIS data had been screened by a quality assurance layer to eliminate bad data before building models, error in atmospheric correction and geometric errors may be present in MODIS data (Vermote and Kotchenova 2008). Fensholt et al. (2010) showed that MODIS red and NIR reflectance were highly dependent on sun-sensor geometry, and NDVI variation was dependent on vegetation density. The MOD09A1 data were not corrected by bidirectional reflectance distribution function (BRDF) to near-nadir reflectance. Both NDVI and NDWI use MODIS band 2 (NIR), so they could be affected by seasonal and interannual variation in viewing geometry (Sims et al. 2011).

An important underlying assumption of upscaling LFMC field sampling to a remote sensing pixel is that remote sensing data are exclusively sensitive to changes in LFMC. In fact, the surface reflectance was an aggregated product of radiative interaction with all features on the landscape within a ground instantaneous field of view (GIFOV). The radiance measured within a MODIS GIFOV is assigned to a 500 m pixel, but can in fact be a measurement of a much larger area depending on viewing geometry. Due to changes in viewing geometry over an orbital cycle, the area measured by a single pixel may not be consistent over time. Even within a single 500 m by 500 m area, vegetation

can be spatially heterogeneous. Many of the 10 sites had multiple vegetation species and complex topography and land cover within a 500 m radius of the site. Changes in features other than the targeted fuel type introduced spectral variation in surface reflectance and challenged successful linkage between LFMC and each remote sensing variable. For instance, the mixed landscape of big sagebrush, Gambel oak and exposed soil at the Black Cedar sites might explain the oddly negative slopes and weak correlations with remote sensing proxies (Figures 2.3 q-s and 2.4 q-s). A final complicating factor for the remote sensing measures is that NDVI, NDWI and CWC are indirectly related to LFMC. NDVI is more closely related to chlorophyll than water content. Variation in chlorophyll content can be caused not only by moisture content, but also plant nutrient deficiency, disease and phenological stages (Bowyer and Danson 2004; Ceccato et al. 2002). NDWI and CWC have stronger connections to water content but do not explain dry matter variation that is a part of the LFMC equation (Serrano et al. 2000). CWC was computed by the method developed by Trombetti et al. (2008). The ANN inversion algorithm used by Trombetti et al. (2008) grouped vegetation into shrubland, forest, and grassland classes. This simplified classification might not describe landscape diversity in my sites.

Most major changes in LFMC are associated with physiological activities of vegetation in response to meteorological conditions and phenology. Big sagebrush starts leaf and stem growth in the spring when temperatures are warm and soil moisture is high. Growth will continue until weather is too hot or soil moisture becomes too low to support transpiration. If moderate temperate and precipitation are present in late summer or early fall, sagebrush may produce a second flush of new growth, although at a smaller scale compared to spring. The surge of LFMC in the spring, decline during the summer and

possible increase in the fall is dependent on the timing and amplitude of moisture availability. Under water stress, sagebrush will express morphological plasticity, including shedding spring leaves, allocating more biomass to vegetative versus reproductive shoots, leaves versus stems, and perennial versus ephemeral leaves. In contrast, new growth of Gambel oak generally starts in late spring and continues until late summer or early fall when soil moisture is a limiting factor. Variation in plant phenology and adaption to moisture availability needs to be accounted for at all levels, from LFMC sampling through remote measurement.

2.6 Conclusions

This paper examined using soil moisture and remote sensing proxies for estimating LFMC in big sagebrush and Gambel oak. Soil moisture is a point-based, continuous measurement of drought condition *in situ*. My results demonstrated that soil moisture can provide better predictive power than remote sensing measures across multiple sites and two species. It can potentially provide an alternative means for LFMC estimation with more frequent temporal coverage, and a soil moisture network could complement LFMC field sampling. Remote sensing measures proved to be less strongly correlated with LFMC data, but provided superior spatial coverage. To make the remote sensing proxies more accurate for operational management, selection of high quality MODIS data with BRDF correction and more homogeneous sampling sites may improve relationships. Seasonality and interannual variation need to be considered in generalized models of pooled data.

CHAPTER 3

SPECTROSCOPIC ANALYSIS OF SEASONAL CHANGES IN

LIVE FUEL MOISTURE CONTENT AND LEAF DRY MASS

3.1 Introduction

Live fuel moisture content (LFMC) is regarded as an important fuel property for determining fire ignition probability (Deeming et al. 1978), fire spread rate (Rothermel 1972), fire occurrence (Chuvieco et al. 2009), fire size (Chuvieco et al. 2009), fire season timing (Dennison and Moritz 2009; Dennison et al. 2008), and fire propagation behavior (Plucinski et al. 2010; Weise et al. 2005). LFMC is measured by oven drying fresh field samples until all moisture has evaporated, and calculating the water content by the mass differences between fresh (m_f) and dried (m_d) samples (Lawson and Hawkes 1989; Pollet and Brown 2007):

$$LFMC = \frac{m_f - m_d}{m_d} \qquad \text{(Equation 3.1)}$$

Field sampling measures LFMC for a specific species at a single site and time, and it is difficult to extrapolate values to larger regions and longer periods. Remotely sensed data have the ability to improve temporal and spatial monitoring of LFMC (Yebra et al. 2013). A number of studies have used empirical methods based on vegetation indices (Dennison et al. 2005; García et al. 2008; Peterson et al. 2008; Qi et al. 2012; Roberts et al. 2006; Stow et al. 2006). Many of these empirical studies have relied on

indices calculated from spectral features not associated with water absorption. Gravimetric water and dry mass measurements can be divided by leaf area to create metrics such as equivalent water thickness (EWT) and dry matter content (DMC). LFMC can be calculated as the ratio of EWT to DMC, and radiative transfer modeling (RTM) can be used to estimate EWT and LFMC (Jurdao et al. 2013; Trombetti et al. 2008; Yebra and Chuvieco 2009; Zarco-Tejada 2003). Leaf spectroscopy approaches for estimating LFMC have included first derivative spectra (Curran et al. 1992), spectral indices (Colombo et al. 2008; Datt 1999; Maki et al. 2004; Peñuelas et al. 1997; Stimson et al. 2005), artificial neural networks (Dawson et al. 1998), RTM inversion (Riaño et al. 2005), continuous wavelet analysis (Cheng et al. 2011), and PLSR (Li et al. 2007).

One challenge in spectral estimation of LFMC is decoupling water and dry mass absorption features in fresh leaf reflectance (Fourty and Baret 1997; Riaño et al. 2005). Biochemical components in dry matter include lignin, cellulose, starch, sugar, and protein; these components and water have absorption features in the near infrared (NIR: 700-1400 nm) and short-wave infrared (SWIR: 1400-2500 nm) (Ceccato et al. 2001; Danson and Bowyer 2004; Fourty et al. 1996). Water absorption usually masks dry matter absorption in the SWIR due to water's higher specific absorption coefficients and frequently greater mass. Kokaly and Clark (1999) and Tian et al. (2001) reported that spectral variation in the SWIR induced by increasing LFMC showed not only a decrease in the amplitude of reflectance due to water absorption, but also changes in the depth and shape of absorption near 1730 and 2100 nm attributed to dry mass. Several studies have compared the estimation of EWT and LFMC using RTM simulation and leaf spectroscopy (Cheng et al. 2011; Colombo et al. 2008; Datt 1999; Maki et al. 2004),

illustrating that LFMC was more difficult to estimate than EWT due to difficulty in estimating DMC. Riaño et al. (2005) obtained poor estimation of LFMC in 37 species due to high uncertainty in the estimation of DMC using a PROSPECT model inversion. DMC was estimated using dry leaves and assumed constant throughout the season. However, plant physiology research has indicated dry mass may not be seasonally constant, and LFMC may change in response to trends in both water and dry mass. For example, Kozlowski and Clausen (1965) studied LFMC and dry mass of leaves and buds for several gymnosperms and angiosperms in the 1963 growing season. The seasonal decrease of LFMC was traceable primarily to increase in leaf dry mass than to decrease in actual water content. More recently, Jolly et al. (2014) found that changes in lodgepole pine moisture content were driven by seasonal changes in foliage dry mass allocation instead of water content. These studies contradict that stable dry mass can be assumed for remote sensing estimation of LFMC.

Several recent studies have explored spectroscopic analysis of dry mass. The leaf mass per area (LMA, equivalent to DMC) has been examined using spectral indices (Féret et al. 2011; le Maire et al. 2008; Wang et al. 2011), PLSR (Asner and Martin 2008; Asner et al. 2011; Doughty et al. 2011), PLSR coupled with variable selection methods (Serbin et al. 2012), Bayesian model averaging (Zhao et al. 2013), and continuous wavelet analysis (Cheng et al. 2014). Most of these models were derived from samples across multiple species collected at discrete times, and the remote sensing literature has not investigated the spectral expression of continuously measured temporal variation in dry mass. It is not clear how the individual biochemical components that make up dry mass change over time and how reflectance spectra respond to combined changes in

water mass, dry mass, biochemical components, and structural changes.

This article addresses the knowledge gap of spectral-temporal response of LFMC and leaf dry mass over the growth season. I seek to answer the following research questions: (i) How do LFMC and dry mass change during the growth season? (ii) How do biochemical components in dry mass contribute to LFMC change and covary over time? (iii) How are changes in leaf spectra over time correlated with changes in LFMC and dry mass? To answer these questions, this study examined seasonal changes in LFMC, dry mass, and leaf spectra of two important species in the western US, sagebrush and lodgepole pine. This analysis evaluated multivariate PLSR models for identifying spectral features correlated with temporal variation in LFMC, dry mass, and biochemical components. Finally, I discuss the physiological interpretation of temporal variation in spectra and make recommendations to the remote sensing and fire research communities.

3.2 Data and Methods

3.2.1 Study Sites and Sampling Design

I collected LFMC samples at four sites near Missoula, Montana between May and October 2012 for two common species in the western US, lodgepole pine (*Pinus contorta* Douglas ex Loudon), an evergreen conifer species, and big sagebrush (*Artemisia tridentate* Nutt), a semideciduous broadleaf shrub species. The two lodgepole pine sites were in natural conifer forest on south slopes at elevations averaging 1330 and 1590 m. The two sagebrush sites were on flat natural shrubland adjacent to mixed conifer forests at elevations of 1133 and 1226 m. All sites represented relatively homogenous patches of the sampled species and spanned a geographic region approximately 558 km2 in size.

The study period started with rainfall in late May, followed by a dry-down period during the summer, and ended with observed precipitation after the middle of October (Figure 3.1). Terminal buds of lodgepole pine started to break in late May, and the elongation of new needles continued until October. New sagebrush leaves flushed in the spring at the tips of branches. New sagebrush leaf blades expanded early during the growing season and later became fragile, and some leaves abscised during prolonged periods of water stress.

I sampled four sites once per week using a random sampling scheme to span a large range of individual trees and shrubs within each study site. Current year ("new") and second year and older ("old") lodgepole pine needles were sampled separately. Due to the difficulty of discriminating first year leaves and older leaves for sagebrush, I collected sagebrush branch tips (3-5 cm) to create one mixed-age sample. I collected about 40 g of needles/leaves from each site on each sampling day. Samples were mixed, and stored in sealed plastic bags in a cooler with ice. Leaves for spectroscopy, LFMC, and biochemical analysis were taken from the same mixed sample pool.

3.2.2 LFMC and Biochemical Measurements

LFMC was measured for 12 groups of 5 needle fascicles from each age group and 12 sagebrush branch tips at each site per sampling day. Fresh mass was determined within 4 h after collection, and then samples were dried in a convection oven for 24 h at a temperature of 95 Celsius degreeand re-weighed. The difference between fresh mass and dry mass was used to determine water mass, and LFMC was calculated using equation 3.1. Dry mass percentage (DMP), the ratio of dry mass to fresh mass, was calculated to

(a)

(b)
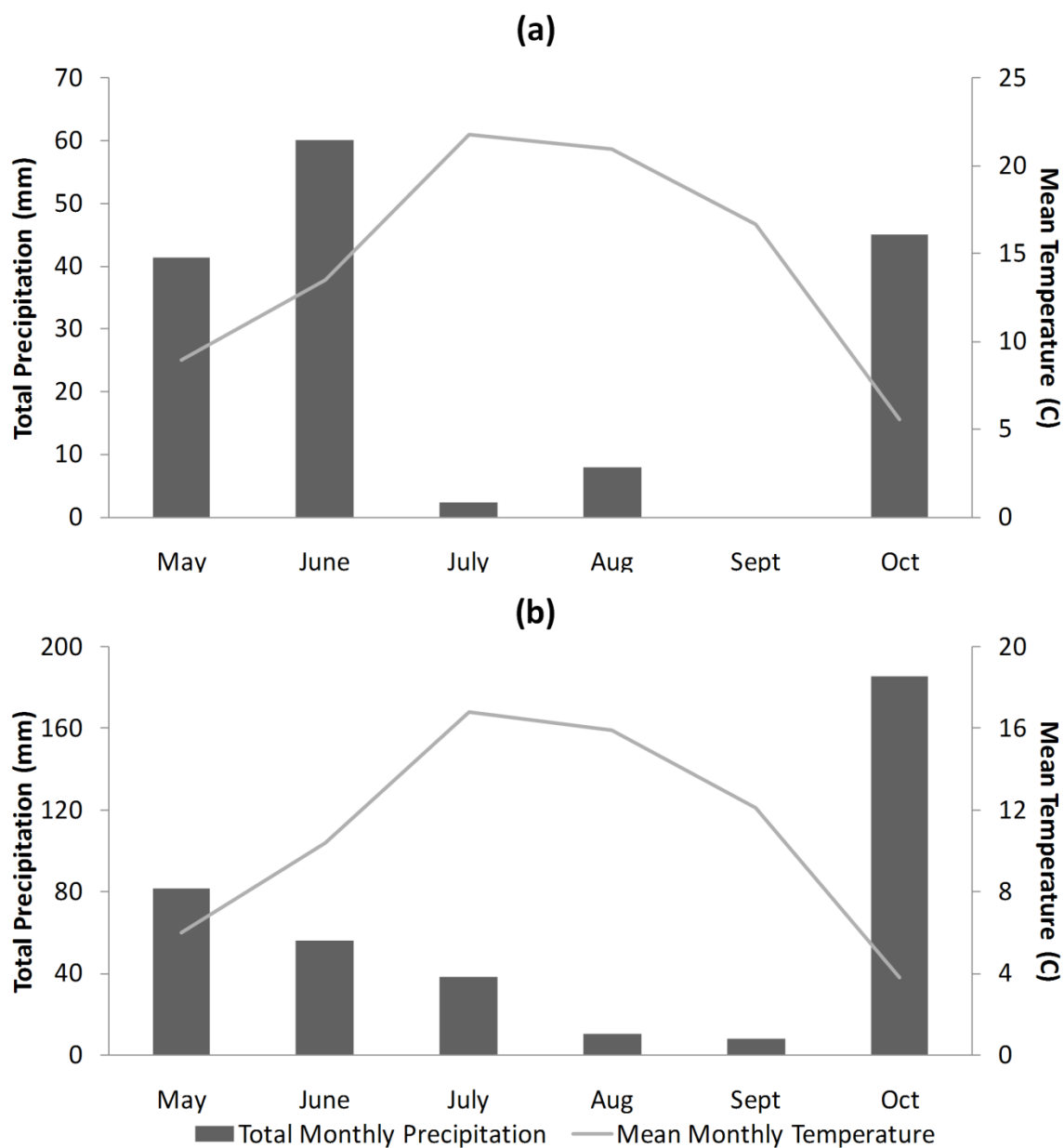
Figure 3.1 2012 plots for weather stations proximate to sagebrush (a) and lodgepole pine (b) sites. Precipitation for (a) was measured at a station an average of 4 km north of the two sagebrush sampling sites, while temperature for (a) was measured at a station 500 m higher in elevation and 7 km to the south of the sampling sites. Precipitation and temperature (b) were measured at lodgepole pine site 2, approximately 12 km to the south of lodgepole pine site 1. (http://www.ncdc.noaa.gov/cdo-web/, last accessed in May, 2014).

track the proportional change of dry mass (Equation 3.2). Relative water content (RWC) is commonly used to assess the water status of plants (Barrs and Weatherley 1962) and has been estimated by spectral data (Serrano et al. 2000). RWC was measured by first recording the fresh mass, recording the turgid mass (m_t) after immersing the needles or leaves in deionized water for 24 hours, and then oven drying the samples for 24 hours to obtain a dry mass (Equation 3.3).

$$DMP = \frac{m_f - m_d}{m_f} \qquad\qquad \text{(Equation 3.2)}$$

$$RWC = \frac{m_f - m_d}{m_t - m_d} \qquad\qquad \text{(Equation 3.3)}$$

Approximately 20 g of the sample were used to further partition dry mass into biochemical components by AgriAnalysis Forage Analysis Laboratory (http://www.agrianalysis.com/, last accessed in May, 2013). Wet chemistry analysis was used to determine neutral detergent fiber (NDF), nonstructural carbohydrate (NSC), neutral detergent soluble fiber (NDSF), protein, fat, and ash as a percentage of dry mass (Table 3.1). NDF includes lignin, cellulose and hemicellulose. Lignin is a complex chemical compound and mainly used in the secondary cell walls of xylem and sclerenchyma. Cellulose is an end product of carbohydrates produced by plant photosynthesis, and it is used for the wall of parenchyma cells in plant leaves. NSC is mainly starch and sugar supplying energy to support respiration. NDF and NSC are usually the two most abundant components of dry mass.

3.2.3 Spectroscopic Measurements

All spectroscopic data were measured using an Analytical Spectral Devices FieldSpec4 High-Res spectrometer (380 – 2500 nm) and an integrating sphere (model

Table 3.1 Description of biochemical components.

Name	Abbreviation	Description
Neutral detergent fiber	NDF	lignin, cellulose, hemicellulose
Non-structural carbohydrate	NSC	sugar, starch
Neutral detergent soluble fiber	NDSF	pectin, β-glucan, galactan, fructan
Protein	N/A	nitrogen bearing content, rubisco
Fat	N/A	isoprenoid, essential oil, wax and other lipid
Ash	N/A	mineral content

RTS-3ZCR2) in a darkroom within 24 hours after sample collection. Measurements used

Daughtry's method (Daughtry et al. 1989) with revision by Mesarch (Mesarch et al.

1999) to measure small leaves. Pine needles and sagebrush leaves were laid side by side

to form a flat mat and taped to a sample holder. Reflectance and transmittance were

measured for the mat using the integrating sphere. Leaf samples were subsequently

scanned with a flatbed scanner at resolution of 1200 dpi. Gap fraction was retrieved from

grayscale scanned images as the ratio of the number of white pixels (gaps) to the total

number of pixels within the mount aperture (Di Vittorio 2009; Rautiainen et al. 2012).

Leaf reflectance was then derived from the mat measurements by correcting for the gap

fractions between leaves:

$$\rho = \frac{\rho_{total}}{1-GF} \qquad \text{(Equation 3.4)}$$

where ρ_{total} is the reflectance of the flat sample mat, GF is gap fraction, and ρ is the

single leaf reflectance. New and old lodgepole needles were measured separately. Since

there is a reported discrepancy between needle adaxial and abaxial optical properties due

to needles' curved shape (Middleton et al. 1997), reflectance and transmittance were

measured on both sides of the needle surface for each sample and averaged. I calculated average reflectance spectra of eight samples for new lodgepole pine needles, old needles, and sagebrush leaves for each observation date. Raw reflectance spectra for each date were convolved to five nm bandwidths. This bandwidth was selected based on the full width-half maximum of the Airborne Visible/Infrared Imaging Spectrometer Next-Generation (AVIRIS-NG) instrument (Kampe et al., 2010). Four hundred and twenty-five spectral bands spanning the 380 – 2500 nm wavelength range were subset to 248 bands by deleting atmospheric water vapor absorption bands at 1340 -1495 nm and bands longer than 1800 nm due to poor performance of the integrating sphere, producing low signal-to-noise ratio beyond this wavelength.

3.2.4 Statistical Analysis

To understand major variation among all measurements during the growth season, I first pooled all data in the sampling period and used principle component analysis (PCA) to determine common seasonal variation in biochemical components and LFMC. In addition, I conducted semipartial correlation analysis to investigate how water and dry mass contribute to LFMC variation. Semipartial correlation estimates the relationship between a predictor variable and an outcome variable while removing the effects of other predictors. Since LFMC is controlled by water mass and dry mass, this method can separate their contributions to temporal variability in LFMC.

I used partial least squares regression (PLSR) to examine temporal variation in spectra correlated with temporal variation in LFMC and biochemical components. PLSR is a particular type of multivariate statistical method widely used in chemometrics and

NIR spectroscopy for analyzing quantitative relationships between multiple predictor and response variables (Martens and Naes 2001). The typical PLSR model includes one response variable at a time, for example, LFMC, and uses spectroscopic data as predictor variables. Multivariate PLSR accounts for the complex correlation between multiple response variables, revealing the relevance of single predictors with regard to individual responses. Since LFMC, dry mass and biochemical components covary over the growing season, I constructed a multivariate PLSR model using all biochemical variables as response variables (normalized before entering the model) and spectroscopic data as predictor variables over the study period. This algorithm handled the correlations between biochemical measurements by projecting correlated response variables to orthogonal components and regressed the components with one set of latent features of predictor variables. Incremental numbers of latent components were tested, and more latent components usually generated higher R-squared values (R^2) and smaller root-mean-square-error (RMSE) but at the risk of over-fitting the data. I reported R^2 and RMSE from PLSR using five components as determined by predictive residual sum of squares (PRESS) analysis (Wold et al. 2001). The regression coefficients of each band over the full wavelength range were analyzed to extract wavelengths sensitive to temporal changes in LFMC and biochemical absorptions.

3.3 Results

3.3.1 Seasonal Variation of LFMC and Biochemical Components

For each species, plot values were averaged and seasonal trends of LFMC and biochemical components were plotted (Figure 3.2). LFMC of new needles was 202% in
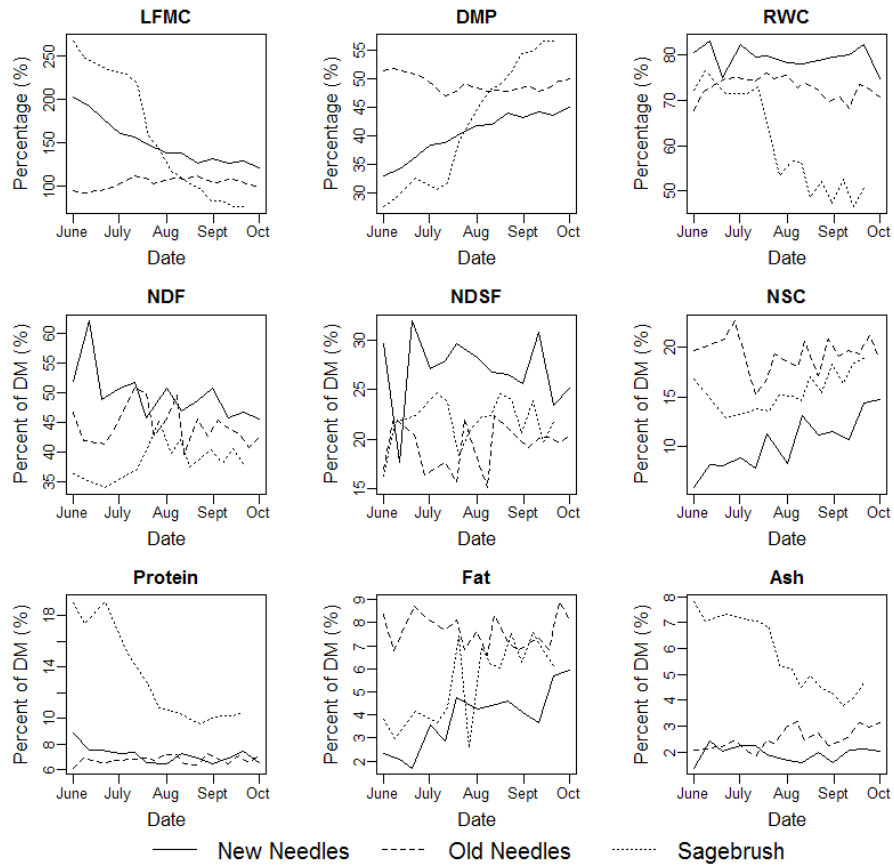
Figure 3.2 Seasonal variation of LFMC, DMP, RWC and biochemical components. For each species, the measurements of two sampling sites were averaged on the observation date.

early June and decreased to 122%, while old needles stayed relatively stable with a slight increase from 93% to 112% in early season. Sagebrush LFMC decreased consistently during the sampling period from 268% to 77%. The DMP of new needles increased from about 35% to 45% and sagebrush increased from about 30% to 55%, while the DMP of old needles dropped slightly from 50% in July and then slightly increased through October. As dry mass accumulated in the new needles, LFMC of new and old needles converged toward late October. The RWC of new and old needles was relatively stable, while in sagebrush RWC decreased over time, demonstrating water stress in August,

September, and October. In sagebrush, NDF and NDSF were relatively stable, but fat content increased while protein and ash content decreased over the study period. The abrupt changes in biochemical components, such as NDSF of new needles in mid-June and fat of sagebrush in late July, were most likely due to measurement errors in wet chemistry analysis. NDF composed the largest percentage of dry mass in both species (Figure 3.3), decreasing from July to September in new and old lodgepole needles, but staying consistent in sagebrush leaves. NDSF and NSC were a smaller fraction of dry mass, with NSC increasing from July to September in all three leaf categories.

PCA analysis showed the temporal covariation among multiple biochemical components (Figure 3.4). Notably, RWC was nearly orthogonal to LFMC and DMP for new needles, while RWC was strongly aligned with these variables in sagebrush. This difference in RWC relationship with LFMC between species reveals a potential difference in water content contribution to LFMC. NSC was directly in opposition to LFMC in the PC1-PC2 space for both new and old needles, demonstrating NSC's strong association with LFMC temporal variation. On the contrary, NSC showed a weaker correlation with LFMC in sagebrush, while ash, protein and fat changed in close response to LFMC. Since LFMC and DMP are complementary measures based on fresh and dry mass, they fell along the same axis of variation but in opposite directions in each plot.

Semipartial correlation analysis provided evidence that dry mass was the dominant driver of LFMC in lodgepole pine needles. Dry mass explained about 37% of the variance in LFMC over time and water mass explained about 5% for new needles (Table 3.2). Dry mass explained 7% more variance of LFMC in old needles than water mass. The covariance between dry mass and water mass explained about 45% of needle
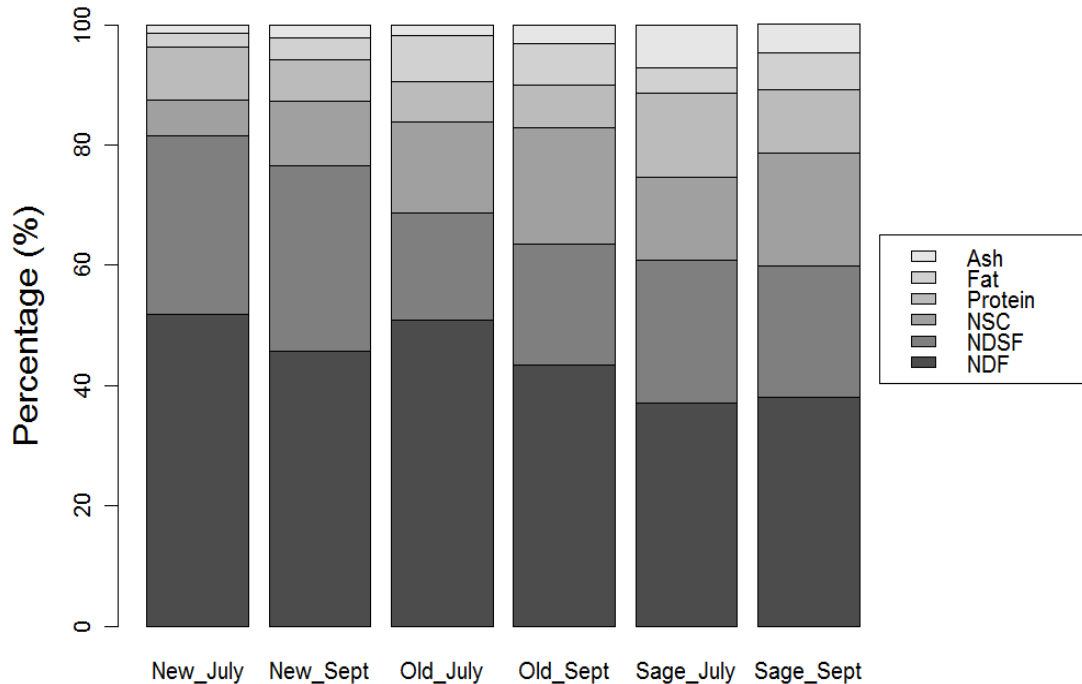
Figure 3.3 Barplot of averaged biochemical components in dry mass of new/old lodgepole pine needles and sagebrush leaves, July and September, 2012.
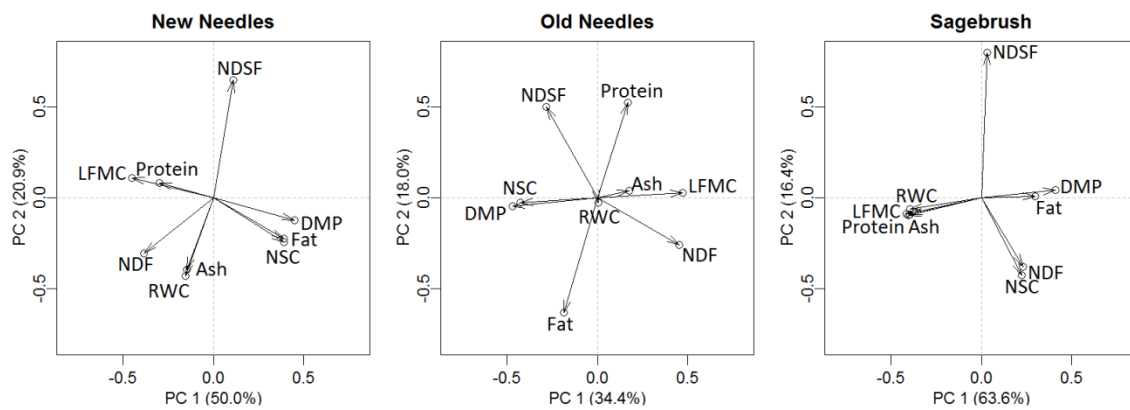
Figure 3.4 Principle component analysis of biochemical components, LFMC and RWC. The percentage in the axis label shows the variance explained by the component.

Table 3.2 Semipartial correlation coefficients of water mass (g) and dry mass (g) in LFMC variation.

Species	Dry Matter	Water	Covariance
New needles	0.37	0.05	0.45
Old needles	0.17	0.1	0.45
Sagebrush	0.24	0.23	0.40

LFMC variation in both new and old needles. Dry mass and water mass showed similar contributions to variation in sagebrush LFMC, while their covariance explained about 40% of variation.

3.3.2 Spectroscopic Analysis

Leaf spectroscopy examined the temporal spectral changes corresponding to variation in LFMC and foliar biochemical composition (Figure 3.5). Comparing July and September, the reflectance of new needles increased across visible, NIR and SWIR (1500-1775 nm) regions as LFMC decreased from 221% to 129%. Changes in visible
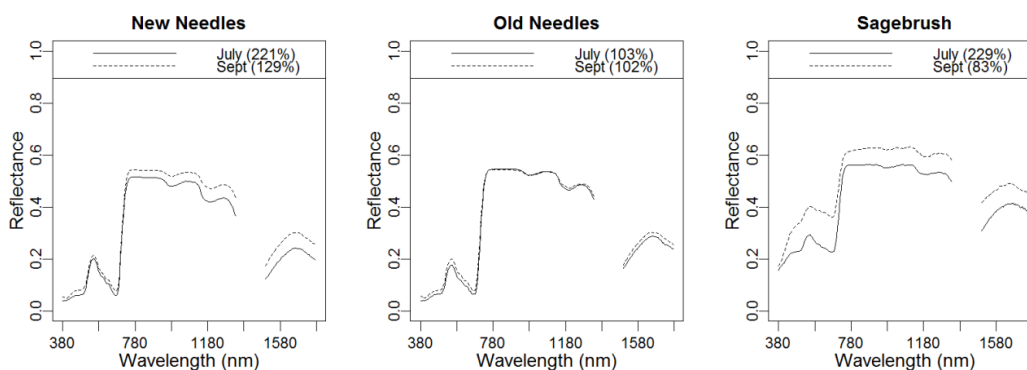
Figure 3.5 Reflectance spectra on two observation dates in July and September for new needles, old needles, and sagebrush leaves. The values in the parentheses were LFMC.

reflectance and water absorption at about 970 and 1200 nm were apparent along with a slight red-edge position shift toward longer wavelength in the NIR. The LFMC of old needles remained stable, but old needles showed slight increases in reflectance in visible bands, near 1200 nm, and in the SWIR. Sagebrush expressed large spectral changes corresponding to LFMC dropping from 229% to 83%. Chlorophyll and water absorption features became weaker causing reflectance to increase, and a weak absorption feature likely associated with dry mass components was expressed near 1700 nm. The red edge shifted towards longer wavelengths between July and September.

PLSR overall showed good estimation for lodgepole pine needle LFMC ($R^2 =$ 0.94 for new needles; $R^2 = 0.72$ for old needles) and DMP ($R^2 = 0.94$ for new needles; $R^2 = 0.75$ for old needles, see Table 3.3). Most biochemical components were accurately estimated in new needles with higher R^2 values for NSC, protein and fat, but the R^2 values were lower than those for LFMC and DMP. Old needles had lower R^2 values for all biochemical components relative to new needles. For sagebrush, LFMC and DMP

Table 3.3 R-squared values (R^2) and root mean square error (RMSE) of partial least square regression between leaf reflectance spectra and scaled biochemical components, LFMC, DMP, and RWC with five latent components. RMSE is in the original unit of each variable: percent for LFMC and DMP, fractional value for RWC, and percent of dry mass for biochemical components.

	New Needles		Old Needles		Sagebrush	
	R^2	RMSE	R^2	RMSE	R^2	RMSE
LFMC	0.94	5.84	0.72	3.51	0.91	21.03
DMP	0.94	1.00	0.75	0.01	0.94	3.00
RWC	0.15	0.03	0.43	0.03	0.85	0.04
NDF	0.57	2.98	0.28	2.92	0.43	2.41
NDSF	0.25	3.20	0.18	2.29	0.08	3.03
NSC	0.72	1.38	0.33	1.61	0.52	1.48
Protein	0.72	0.32	0.42	0.32	0.87	1.22
Fat	0.82	0.57	0.32	0.73	0.58	1.19
Ash	0.6	0.18	0.53	0.30	0.87	0.48

showed comparable R^2 but higher RMSE than models of new needles (RMSE = 21.03 for LFMC, RMSE = 3.00 for DMP). Biochemical component models showed the highest R^2 values for protein and ash. Spectroscopic data explained about 85% variance in sagebrush RWC, much higher than 15% in new needles and 43% in old needles.

    I constructed multivariate PLSR models on pooled data for each species and compared coefficients between response variables (Figure 3.6). The coefficients showed to what magnitude a spectral region is associated with seasonal changes in LFMC and dry mass. In lodgepole pine, PLSR identified common wavelength ranges across most biochemical variables, with high coefficients located near the green reflectance peak (550
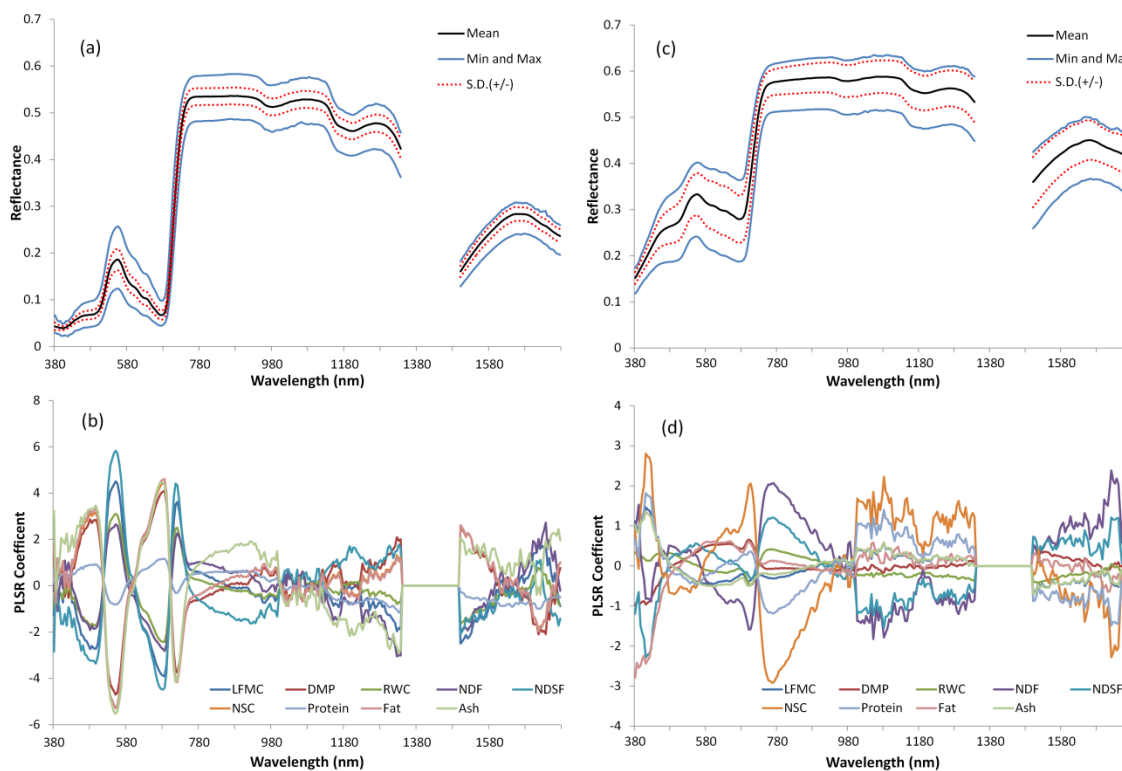
Figure 3.6 Spectral mean, standard deviation, and range over the season (a and c) and coefficients of partial least square regression models (b and d). (a-b) Pooled lodgepole pine new and old needles; (c-d) pooled big sagebrush leaves.

nm), near chlorophyll absorption bands (450 and 650 nm), and near the red-edge in the NIR (710 nm). Sagebrush showed common high coefficients across most biochemical variables around 430 nm, at the red-edge (710 nm), in NIR regions associated with structural scattering (750-800, 1000-1100 nm), and dry matter-associated absorption peaking near 1720 nm. Water absorption regions were also highlighted with higher coefficients near 980 and 1245 nm.

3.4 Discussion

Seasonal changes in foliar biochemical components explained the physiological foundations of LFMC variation. Simple carbohydrates are produced by photosynthesis and converted into new protoplasm and cell wall by the existing protoplasm (Kramer and Kozlowski 1960). In many evergreen species the old needles supply carbohydrates for expansion of the new growth (Kozlowski 1964). Dry weight of gymnosperm old needles significantly decreased when new shoots were expanding. Early field studies in *Pinus resinosa* (Kozlowski and Clausen 1965) and *Pinus sylvestris* (Rutter 1957) have demonstrated this mechanism. In this study, the NSC increased in new needles as they expanded, and peaked toward the end of the October. NSC increased markedly in old needles during the spring. Immediately after the rapid new growth in early July, old needle NSC declined (Figure 3.2). Thus, increase in NSC in new needles was associated with a temporary decrease in NSC in older foliage. New growth supplies an increasingly larger share of the carbohydrates used in their growth toward the end of their expansion period, thus they depend progressively less on imported carbohydrate from older needles. Near the end of the period of needle elongation, new needles continued to develop

structurally, and older needles regained dry mass. Bansal and Germino (2009) observed similar NSC temporal patterns in several montane conifer species in the Rocky Mountains, USA. The semipartial correlation analysis provides statistical evidence that dry mass is a more important factor than water content for determining LFMC variation in lodgepole pine needles. New and old needle RWC stayed relatively stable over the season, confirming that water content is not likely to be driving changes in LFMC. In comparison, sagebrush showed decreasing LFMC, increasing DMP, and a substantial drop in RWC, which corresponded to a consistent dry-down pattern during the summer and a reflush in early August due to a short period of precipitation.

Leaf reflectance spectra are determined by leaf surface properties, internal structure, and the concentrations and distributions of leaf biochemical components (Peñuelas and Filella 1998). Changes in leaf structure and biochemistry occur seasonally. Photosynthetic pigments (mainly chlorophyll a and b) in new foliage increase from the spring to the late growth season (Demarez et al. 1999; Gond et al. 1999; Zhang et al. 2008), resulting in changes of absorption features in the visible region. Leaf morphology, including LMA, leaf thickness, and leaf density, changes with leaf development (Mediavilla et al. 2011). I found seasonal changes in new pine needle morphology including needle thickness, length, width and density (unpublished data). Gradually increasing needle thickness and density is associated with increased NIR reflectance. The variation in leaf pigment and leaf structure was also expressed through seasonal trends in red-edge characteristics (Miller et al. 1991). Water and biochemical components in dry matter changed concurrently with plant physiological processes and confounded time-series absorption and scattering features in the SWIR (Stuckens et al. 2011). Seasonal

trends in pigment absorption and needle morphology expressed through visible and NIR reflectance were apparently stronger than the expression of changes in biochemical components expressed in the SWIR.

Numerous spectral features ranging from the visible to the SWIR have been found to be correlated with LFMC. Previous studies have found that indices not based on water absorption nor on dry matter absorption (e.g., normalized difference vegetation index and visible atmospherically resistant index) are correlated with seasonal variation in LFMC (e.g., Stow et al. 2006; Qi el al 2012). Several spectroscopic analyses of LFMC have highlighted wavelengths ranging from the visible to the SWIR. Li et al. (2007) used genetic algorithm partial least squares regression (GA-PLSR) to model LFMC in 49 samples of 37 species, and the model selected spectral regions around the green peak (517-606 nm), near-infrared plateau (720-740 nm), and SWIR regions beyond 1350 nm. The selection of green peak and NIR bands reflected a correlation between chlorophyll-a and LFMC. Cheng et al. (2011) modeled LFMC with continuous wavelet analysis (CWA) in 265 samples of 47 species in tropical forest, highlighting two features on the leading edge of water absorption bands and four features in SWIR accounting for the depth and width of dry matter absorption. Their analysis showed that more LFMC information was captured by the variation in depth and shape of dry matter absorptions than by changes in water absorption features. In my study, PLSR coefficients of LFMC in two species generally indicate higher weightings across broad spectral regions in the visible, red-edge, and NIR (Figure 3.6). Relatively lower PLSR coefficient weightings are located at water and dry mass absorption regions for lodgepole pine, while sagebrush did have higher weightings in these absorption regions. My study is unique from previous studies in that I

examined multitemporal fresh leaf spectroscopy of the same species. Although leaf dry mass increases in new lodgepole pine needles drive LFMC to decrease, dry matter absorption in the SWIR is not the dominant feature in seasonal reflectance trends. The highlighted visible region is associated with chlorophyll absorption, and the red-edge and NIR regions are correlated with leaf structural changes (Miller et al. 1991).

Previous studies using leaf spectroscopy to estimate field sampled LFMC showed significantly different accuracy across species, which was partially attributed to poor estimation of dry mass (Cheng et al. 2011). Recent studies have used spectroscopic data to estimate leaf mass per area (LMA). Asner et al. (2011) identified that NIR and SWIR contributed the most to reflectance-based estimates of LMA in tropical forest species, especially between 1300 and 2400 nm. Cheng et al. (2014) determined two major wavelet features at 1639 and 2133 nm for predicting LMA. Serbin (2012) used variable selection method with PLSR to predict LMA and selected wavelengths in visible, NIR and SWIR. These studies are based on aggregated datasets from multiple species, and show potential differentiation of leaf dry mass between species. Continuing on these efforts, my research is an assessment of the utility of PLSR models to track temporal leaf dry mass change and individual biochemical components. The novel result of this study is that spectroscopy combined with PLSR can estimate seasonal variation in leaf dry matter (DMP) at high accuracy, but this result is due to broad spectral changes rather than specific absorption features associated with each component of dry matter. The strong spectral features located in visible and NIR regions were given high weightings for most biochemical components, showing general agreement with previous studies. Lignin and cellulose (NDF) was the most abundant constituent in dry leaf matter accounting for 49%

of new needles, 44% of old needles, and 39% of sagebrush leaves. Coefficient weightings near 1720 nm, associated with lingo-cellulose absorption, were high for sagebrush and indicated increased expression of this absorption feature as LFMC declined over time. Stronger expression of NDF beyond 1800 nm may have produced more spectrally distinct features for lodgepole pine and sagebrush, but unfortunately, this spectral range was not measureable using the RTS-3ZCR2 integrating sphere.

My study demonstrates that spectroscopic techniques may be capable of monitoring seasonal variation in LFMC, but that spectral changes over time may be weakly linked to actual water content in some species. Temporal changes in spectra and PLSR coefficients indicate that pigments, leaf structure, water and dry mass may all have coinciding temporal trends that are correlated with LFMC trends. Temporal trends in a single variable, such as water content or a single biochemical component, may be difficult to separate using spectral information due to these coinciding temporal trends. Several authors have combined band selection methods with PLSR to identify bands sensitive to LFMC (Li et al. 2007) and LMA (Serbin et al. 2012), but PLSR coefficients may select bands that are not directly caused by water content or dry mass absorption. My study makes further efforts to investigate the utility of PLSR for modeling multitemporal changes. Accurate estimation of LFMC in conifer species like lodgepole pine calls for careful wavelength selection, since water absorption bands may not capture seasonal trends and less prominently expressed dry matter may be responsible for most of the temporal variability in LFMC.

3.5 Conclusions

Leaf spectra, LFMC, DMP, RWC, and biochemical components measured over a May-October study period revealed substantial covariation. New and old lodgepole pine needles showed distinctly different seasonal trends in LFMC, with old needles presenting little change over time. Biochemical measurements illustrated the underlying foundation of LFMC variation, and dry mass appears to be a more important driver of LFMC variation than water in lodgepole pine needles. Water and dry mass had similar contributions to LFMC variation of sagebrush. These findings coincide with previous plant physiological studies for several conifer species and challenge the assumption of stable dry mass and leaf structure used in RTM retrieval of LFMC. Lodgepole pine and many conifer species can retain multiple years of needles, and new needle growth will influence LFMC of the whole canopy. Since much of the canopy reflectance signal should come from new needles at the branch tips, the complexity of temporal variation in dry mass should make the remote estimation of LFMC at the canopy scale more difficult. My PLSR analysis showed good estimation of temporal trends in LFMC and dry mass. PLSR coefficients for LFMC and dry mass tended towards high weightings for broadly attributable spectral features rather than to discrete absorption features produced by dry matter. While choosing correlated wavelength (such as visible and NIR bands) can indirectly predict LFMC variation, accurate estimation of dry matter remains an important step toward better temporal LFMC monitoring.

LFMC and many biochemical components could be modeled by PLSR and spectroscopic data with reasonable accuracy. My multivariate PLSR model provided new insights by taking into consideration the multilinearity between dependent variables in

order to isolate spectral signals to a single constituent. Identified spectral features were broad and likely dominated by changes in chlorophyll absorption and structural attributes, and in the case of sagebrush, changes in water content. Fresh leaf spectroscopy is valuable for estimating collective trends in dry matter and LFMC, but might not be efficient for modeling individual components of dry mass due to complex interdependence. Future work will need to examine how foliar spectral signatures of LFMC and dry matter are confounded by canopy structure, leaf area index (LAI), soil backscattering and vegetation fraction at the canopy scale.

LFMC has been a foundational component of the past 40 years of scientific work on fire behavior. Previous studies assumed LFMC to represent the changing water content of fuels, while fuel loading (i.e., dry mass) remains stable over time. My study has demonstrated strong seasonal trends in dry matter variation. Accurate remote estimation of LFMC is likely possible for many species based on strongly correlated trends in visible, NIR, and SWIR reflectance. However, remotely observed changes in LFMC should be regarded cautiously for species with terminal new growth, such as lodgepole pine. Temporal trends in LFMC for some species may not indicate the "dry down" signal of water frequently attributed to decreasing LFMC, and may have important departures from the assumption of constant dry mass used for LFMC in fire behavior modeling.

CHAPTER 4

REMOTE SENSING ESTIMATION OF LEAF NET HEAT CONTENT

FOR IMPROVED ESTIMATION OF FIRE BEHAVIOR

4.1 Introduction

Wildfire is a significant disturbance in the terrestrial biosphere. It results in carbon sink-source conversion, long-term alteration of CO_2 flux, and ecosystem function transition (Bowman et al. 2009; Cochrane 2003; Van Der Werf et al. 2006). LFMC is defined as the ratio of water content to dry matter content in live vegetation (Equation 4.1). It is measured by oven drying fresh field samples until all moisture has evaporated, and calculating the water content by the mass differences between fresh (m_f) and dried (m_d) samples (Lawson and Hawkes 1989; Pollet and Brown 2007):

$$LFMC = \frac{m_f - m_d}{m_d} \qquad \text{(Equation 4.1)}$$

The popularity of LFMC as a measure of fire danger stems from its use as an input to the Rothermel (1972) model of surface fire spread rate. Fuel models used in the Rothermel-type fire behavior and fire spread models typically assume that dry mass does not change over time, and the heat content of dry mass is constant over time and across species. However, plant physiology studies have demonstrated seasonal variation in dry mass, such that temporal variation in LFMC can be due to changes in both water mass and dry mass. Kozlowski and Clausen (1965) found the seasonal decrease of LFMC was

traceable primarily to greater increase in leaf dry mass than to decrease in actual water content for several gymnosperms and angiosperms. Chapter 3 found that changes in lodgepole pine LFMC were driven by seasonal changes in foliage dry mass instead of water content. For big sagebrush, water and dry mass had similar contribution to LFMC seasonal change. As a ratio of water to dry mass, the LFMC cannot describe how water or dry mass change individually, resulting in an incomplete proxy of fire danger. A more direct measure of potential heat release by combustion as a function of both water and dry mass could potentially improve both fire behavior and fire danger modeling.

Fire behavior models use fuel models to parameterize different fuel categories as a set of mathematical inputs (Albini 1976; Andrews et al. 2003; Burgan and Rothermel 1984; Finney 1998; Rothermel 1972). The original 13 fuel models used a single value of 18.61 MJ kg^{-1} for heat content in all fuel models. Those fuel models have worked well for predicting surface fire spread rate and intensity of active fires at peak of fire season in part because the associated dry conditions lead to a more uniform fuel complex, an important assumption of the underlying fire spread model (Scott and Burgan 2005). However, the actual heat release from burning fuel varies as the water mass and dry mass change during the season and across fuel types. Several studies have specified heat content variation in a variety of species at greater precision (Dibble et al. 2007; Dimitrakopoulos and Panov 2001; Reid and Robertson 2012; Van Wagdendonk et al. 1998; Williamson and Agee 2002).

Here, I introduce leaf net heat content (LNHC) as a complementary measure of fire danger to LFMC. LNHC is defined as the total heat released by combustion of dry matter subtracted by the heat absorbed for preheating and evaporating water (Equation

4.2). Heat content (HC) is defined as total heat released from combustion per unit dry

$$LNHC = HC - LFMC * (C * \Delta T + H_V) \qquad \text{(Equation 4.2)}$$

mass (J g^{-1}). C is the specific heat of water (4.186 J g^{-1} $^{\circ}$C^{-1}), ΔT is the temperature

change from ambient temperature to 100 $^{\circ}$C, and H_V is the heat of vaporization of water

(2260 J g^{-1}). Since LNHC captures independent effects of both water mass and dry mass,

it is a more direct estimate of combustion energy than LFMC for modeling fire behavior.

LFMC has been the most frequently used measure of fire danger in remote

sensing applications (Yebra et al., 2013), as vegetation reflectance spectra respond to

water and dry matter absorption features. Previous studies have used remotely sensed

vegetation indices (Dennison et al. 2005; García et al. 2008; Peterson et al. 2008; Qi et al.

2012; Roberts et al. 2006) and radiative transfer modeling (Jurdao et al. 2013; Riaño et al.

2005; Trombetti et al. 2008; Yebra and Chuvieco 2009; Zarco-Tejada 2003) to estimate

LFMC. Since LNHC directly associates with leaf water and dry mass, empirical

correlations between vegetation indices and LFMC based on seasonal variation may also

extend to LNHC (Qi et al. 2014; Stow and Niphadkar 2007; Stow et al. 2006). I intend to

answer these research questions: 1) how do LFMC and LNHC change over time; 2) what

is the relationship between LFMC and LNHC; 3) is it possible to remotely estimate

LNHC? LNHC and LFMC were measured using samples from two species over a period

of three months. I also collected leaf-scale lab spectra and MODIS spectra over the same

sampling period. Relationships between LNHC, LFMC, and vegetation indices calculated

from lab and MODIS spectra were analyzed using regression modeling.

4.2 Data and Methods

4.2.1 Study Area

I studied two common species in the western USA, lodgepole pine (*Pinus contorta* Douglas ex Loudon), an evergreen needleleaf tree species, and big sagebrush (*Artemisia tridentate* Nutt), a semideciduous broadleaf shrub species. I collected field samples at two lodgepole pine sites in natural conifer forests and at two big sagebrush sites near Missoula, Montana between July and October, 2012. Current-year pine needles started to emerge in early June and elongated until the end of growth season. Sagebrush started a flush of new leaves in late May. All sites represented relatively homogenous patches of the sampled species and spanned a geographic region approximately 558 km^2 in size, with elevations ranging between 1133 and 1590 m. I sampled all four sites once per week using a random sampling scheme to include a large number of individuals from each species. Current year pine needles and sagebrush branch tips (3-5 cm) were collected to represent new growth. About 40 g of foliage were collected and mixed from each site on the sampling day, and then stored in sealed plastic bags in a cooler with ice. Leaves for measurement of HC, LNHC, LFMC, and spectroscopy were taken from the same mixed sample.

4.2.2 HC, LNHC, and LFMC Measurements

About 0.3 g of oven-dried pine needles and sagebrush leaves were burned in a calorimeter to measure HC (J g^{-1}), and the average of three measurements was recorded for each site for each date. LFMC was measured for 12 groups of 5 needle fascicles and 12 sagebrush branch tips at each site. Fresh mass was determined within 4 hours after

collection, and then samples were dried in a convection oven for 24 hours at a temperature of 95 ºC and re-weighed. The difference between fresh mass and dry mass was used to determine water mass, and LFMC was calculated using equation 4.1. LNHC was calculated using equation 4.2 after pairing HC and LFMC data for each site for the same sampling day. Ambient temperature in equation 4.2 was set as 30 ºC to approximate dry, hot, summer conditions.

4.2.3 Spectroscopic Measurements

I used an Analytical Spectral Devices FieldSpec4 High-Res spectrometer (380 – 2500 nm) and an integrating sphere (model RTS-3ZCR2) to measure leaf-scale spectroscopic data within 24 hours after sample collection. Pine needles and sagebrush leaves were laid side by side to form a flat mat. Measurements used Daughtry's method (Daughtry et al. 1989) with revision by Mesarch (Mesarch et al. 1999) to calculate the reflectance and transmittance of a single needle. For both species I measured reflectance on the adaxial and abaxial surface of leaves and took the mean as the reflectance for one sample. I then measured eight samples on each observation date for each species per site and calculated average reflectance spectra. Raw reflectance spectra were convolved to bands 1-7 of the Moderate Resolution Imaging Spectroradiometer (MODIS).

4.2.4 MODIS Data

I downloaded MODIS NBAR MCD43A4 products from the Oak Ridge National Laboratory MODIS Global Subsets site (http://daac.ornl.gov/cgi-bin/MODIS/GLBVIZ_ 1_Glb/modis_subset_order_global_col5.pl, last accessed in May 2014). MCD43A4 is a

500 m, 16 day aggregated product that approximates a nadir view zenith angle and solar zenith angle for local solar noon. I extracted a single pixel of relatively homogenous species cover centering on or adjacent to each sample site. I excluded one sagebrush site from MODIS scale analysis because the sagebrush cover was less than one pixel for the 500 m pixels surrounding the site. In order to preserve the temporal trend of ground measurements, multiple LNHC and LFMC within each 16-day MCD43A4 observation window were averaged. Cloud and bad band data were masked using the MODIS quality assurance layer.

4.2.5 Vegetation Indices and Statistical Analysis

I calculated a series of vegetation spectral variables using convolved leaf spectra and MODIS data (Table 4.1). These include vegetation greenness indices (NDVI, SAVI, EVI, and VARI) and water indices (NDWI, NDII6, and GVMI), all of which have been used in previous MODIS studies to estimate LFMC (e.g., Caccamo et al. 2012; Dennison et al. 2005; Peterson et al. 2008; Qi et al. 2012; Roberts et al. 2006; Stow et al. 2005). Greenness indices used the red wavelength in the band ratio calculation to account for chlorophyll absorption. The chlorophyll content is correlated with water content so the greenness indices can be used as indirect indicators for LFMC. Water indices used water absorption features in the shortwave infrared to provide a more direct connection to water content.

Since NDVI is prone to soil backscattering effect, SAVI was explicitly designed to correct for background soil brightness (Huete 1988). Huete (2002) introduced EVI to improve sensitivity in high biomass regions and reduce canopy background signal and

Table 4.1 Spectral indices calculated for MODIS including their shortened acronym, mathematical formulation and reference. ρ is reflectance and the subscripts refer to MODIS bands.

Index	Formulation	Reference
Normalized Difference Vegetation Index	$NDVI = \dfrac{\rho_2 - \rho_1}{\rho_2 + \rho_1}$	Rouse et al.(1973)
Soil Adjusted Vegetation Index	$SAVI = (1 + 0.5) * \dfrac{\rho_2 - \rho_1}{\rho_2 + \rho_1 + 0.5}$	Huete (1988)
Enhanced Vegetation Index	$EVI = \dfrac{2.5 * (\rho_2 - \rho_1)}{(\rho_2 + 6 * \rho_1 - 7.5 * \rho_3 + 1)}$	Huete et al. (2002)
Visible Atmospherically Resistant Index	$VARI = \dfrac{\rho_4 - \rho_1}{\rho_4 + \rho_1 - \rho_3}$	Gitelson et al. (2002)
Normalized Difference Water Index	$NDWI = \dfrac{\rho_2 - \rho_5}{\rho_2 + \rho_5}$	Gao and Goetz (1995)
Normalized Difference Infrared Index	$NDII6 = \dfrac{\rho_2 - \rho_6}{\rho_2 + \rho_6}$	Hardisky et al. (1983)
Global Vegetation Moisture Index	$GVMI = \dfrac{(\rho_2 + 0.1) - (\rho_6 + 0.02)}{(\rho_2 + 0.1) + (\rho_6 + 0.02)}$	Ceccato et al. (2002)

atmosphere influences. Although leaf spectra did not have influences from soil and canopy, I still calculated SAVI and EVI in leaf spectra to compare with MODIS spectra. I also calculated canopy water content (CWC) in leaf and MODIS spectra by an inversion of Prospect-SailH radiative transfer model (Jacquemoud et al. 1995; Kuusk 1995) through an artificial neural network (ANN) combined with NDVI and normalized difference indices using 1640 nm and 2130 nm as absorption bands (Trombetti et al.

2008). CWC (expressed in mm) was computed as the product of leaf area index and equivalent water content. CWC was not designed for application to leaf spectra, but was applied to both convolved leaf and MODIS spectra for comparison.

I conducted bivariate linear regression between LFMC, LNHC and remote sensing variables for each site. I reported adjusted R-squared values (R^2_{adj}) and normalized root-mean-square-error (NRMSE) to compare model performance (Equation 4.3). NRMSE gives an indication of actual error without being influenced by the data unit, as is the case for RMSE, allowing for comparison of error between measures with different units such as LFMC and LNHC (Richter et al. 2012).

$$NRMSE = 100 * \frac{RMSE}{Range(observation)}$$
(Equation 4.3)

4.3 Results

Field sampled LFMC, HC, and LNHC values were pooled for each species. LFMC for lodgepole pine needles was 202% in mid-July when new growth started to emerge (Figure 4.1). As the needles developed, LFMC decreased to 121% in mid-October. Sagebrush had high LFMC at 239% at the beginning of the sampling period and dropped to 71% at the end of September. LFMC rate of decrease over time slowed at the end of the sampling period. The HC of pine needles increased from 20226 to 21366 J g^{-1}, and sagebrush increased from 19043 to 20601 J g^{-1} (Figure 4.2). Compared to HC, LNHC showed larger seasonal variation due to the inclusion of a water heat sink. The LNHC of needles was 15057 J g^{-1} in mid-July and increased to 18199 J g^{-1} in mid-October, while sagebrush LNHC increased consistently during the sampling period from 12953 to 18779 J g^{-1} (Figure 4.3).
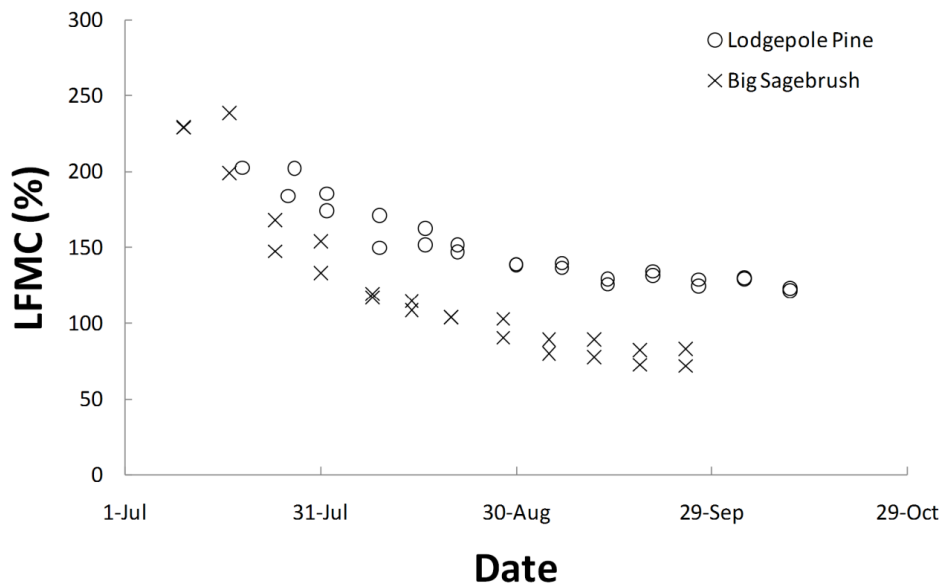
Figure 4.1 Seasonal trends in LFMC for new pine needles and sagebrush leaves.
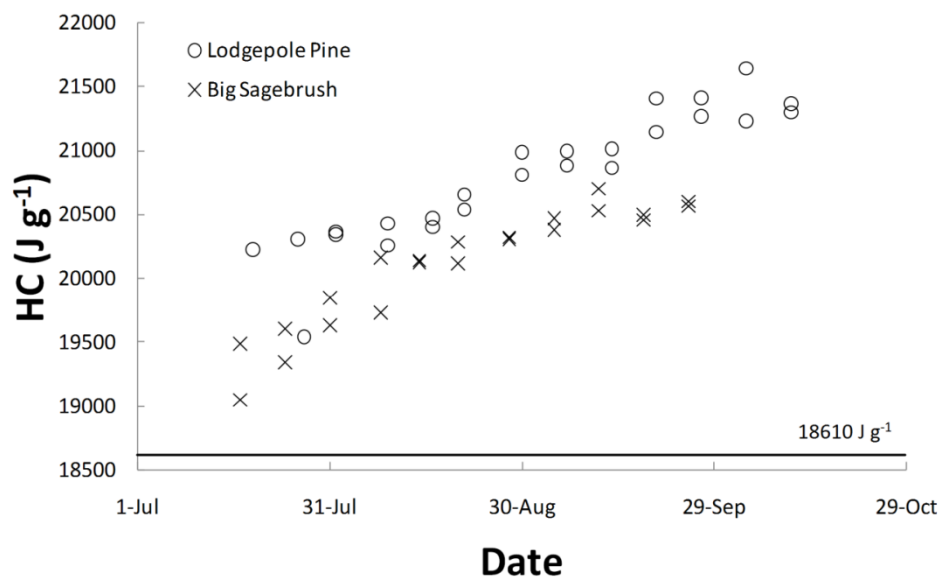
Figure 4.2 Seasonal trends in HC for new pine needles and big sagebrush leaves. The solid line is the standard HC values 18610 J g^{-1} in Albini (1976).
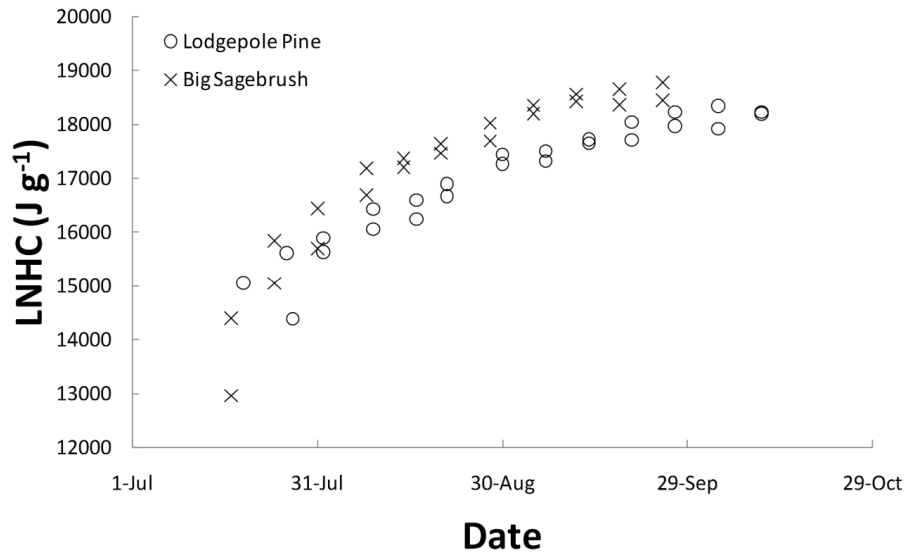
Figure 4.3 Seasonal trends in LNHC of new pine needles and big sagebrush leaves.

LNHC and LFMC were negatively correlated for both species (Figure 4.4). As the LFMC decreased during the season, the LNHC increased to its highest values. The R^2_{adj} of linear regression between LNHC and LFMC was 0.95 for lodgepole pine needles and 0.99 for sagebrush leaves. More importantly, lodgepole pine generally had higher LNHC than big sagebrush when they presented similar LFMC. For example, pine and sagebrush showed 17713 and 16443 J g^{-1} LNHC, respectively, at 133% of LFMC, which was due to the different HC, with 21144 J g^{-1} for pine and 19848 J g^{-1} for sagebrush.

For leaf scale measurements, relationships between vegetation indices and LNHC or LFMC varied by the spectral regions used for each index (Figure 4.5). Greenness indices generally had lower R^2_{adj} and larger NRMSE than water indices in pine needle LNHC models. Three water indices produced comparable R^2_{adj} values with GVMI having the highest R^2_{adj} of 0.68 for LNHC at lodgepole pine site 1. Each index produced comparable NRMSE between LNHC and LFMC with the average difference within 5%.
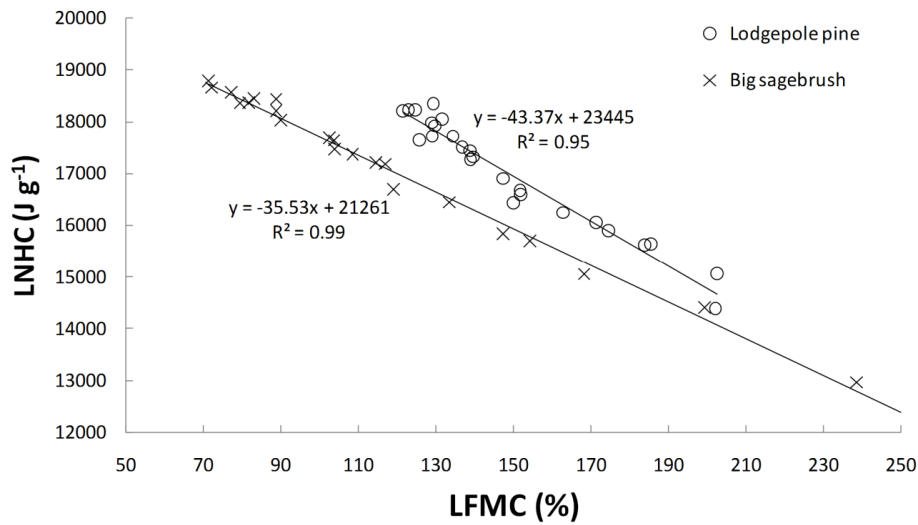
Figure 4.4 Relationships between LFMC and LNHC for new lodgepole pine needles and big sagebrush leaves.
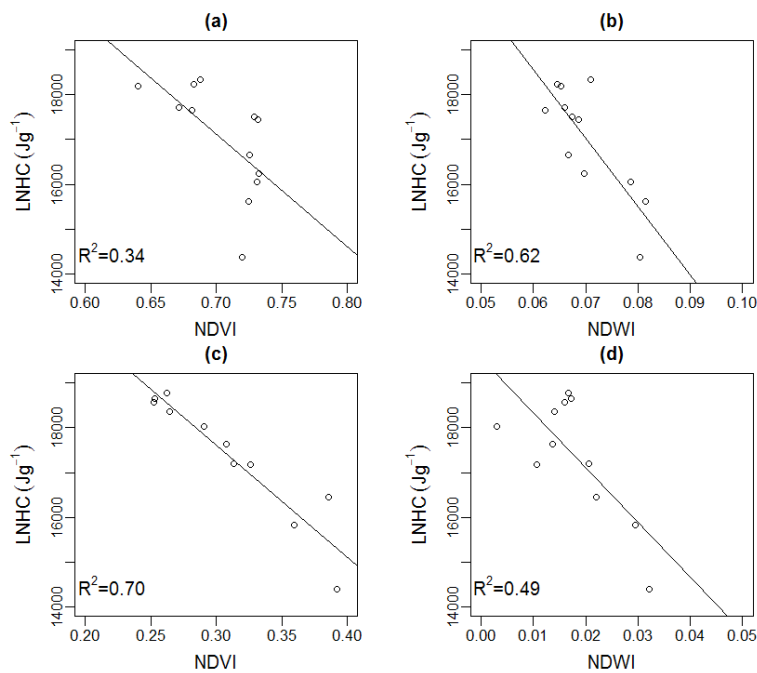
Figure 4.5 Linear correlation between LNHC and NDVI and NDWI at leaf scale. (a-b) Lodgepole pine site 1; (c-d) big sagebrush site 1.

On the contrary, all greenness indices in sagebrush LNHC models showed higher R^2_{adj} values and smaller NRMSE than water indices. The VARI at sagebrush site 2 showed highest R^2_{adj} of 0.88 and smaller NRMSE of 9.93%. Compared to LNHC, all indices in sagebrush LFMC models produced R^2_{adj} values above 0.7. LNHC had smaller NRMSE values in greenness indices and higher NRMSE values in water indices than LFMC models. The RTM-inverted CWC showed weaker correlation with LNHC than vegetation indices at the two lodgepole pine sites. However, CWC performed better for sagebrush sites with the highest R^2_{adj} values of 0.81 in LNHC models. In both species, the R^2_{adj} of greenness indices in LNHC models were similar to or higher than those in LFMC models, but R^2_{adj} of water indices in LNHC models were lower than those in LFMC models. Weak correlation between greenness indices and LNHC at leaf scale showed nonlinear relationships. For example, the NDVI showed little variation when LNHC decreased below 17000 J g^{-1} at lodgepole pine site 1 (Figure 4.6). While in sagebrush NDVI expressed a stronger linear relation with LNHC, NDWI produced higher R^2_{adj} in estimating lodgepole pine LNHC than sagebrush.

For MODIS pixel spectra, the R^2_{adj} of greenness indices in LNHC models increased at two lodgepole pine sites (Figure 4.7). For example NDVI increased from 0.34 to 0.76 at lodgepole site 1 (Figure 4.8). However, the R^2_{adj} values of water indices generally decreased, except NDWI at lodgepole pine site 1. As a result, the greenness indices outperformed water indices in estimating LNHC of lodgepole pine, and LNHC models generally similar to or higher R^2_{adj} than LFMC models. At the sagebrush site, both greenness and water indices produced higher R^2_{adj} of LNHC in MODIS pixel
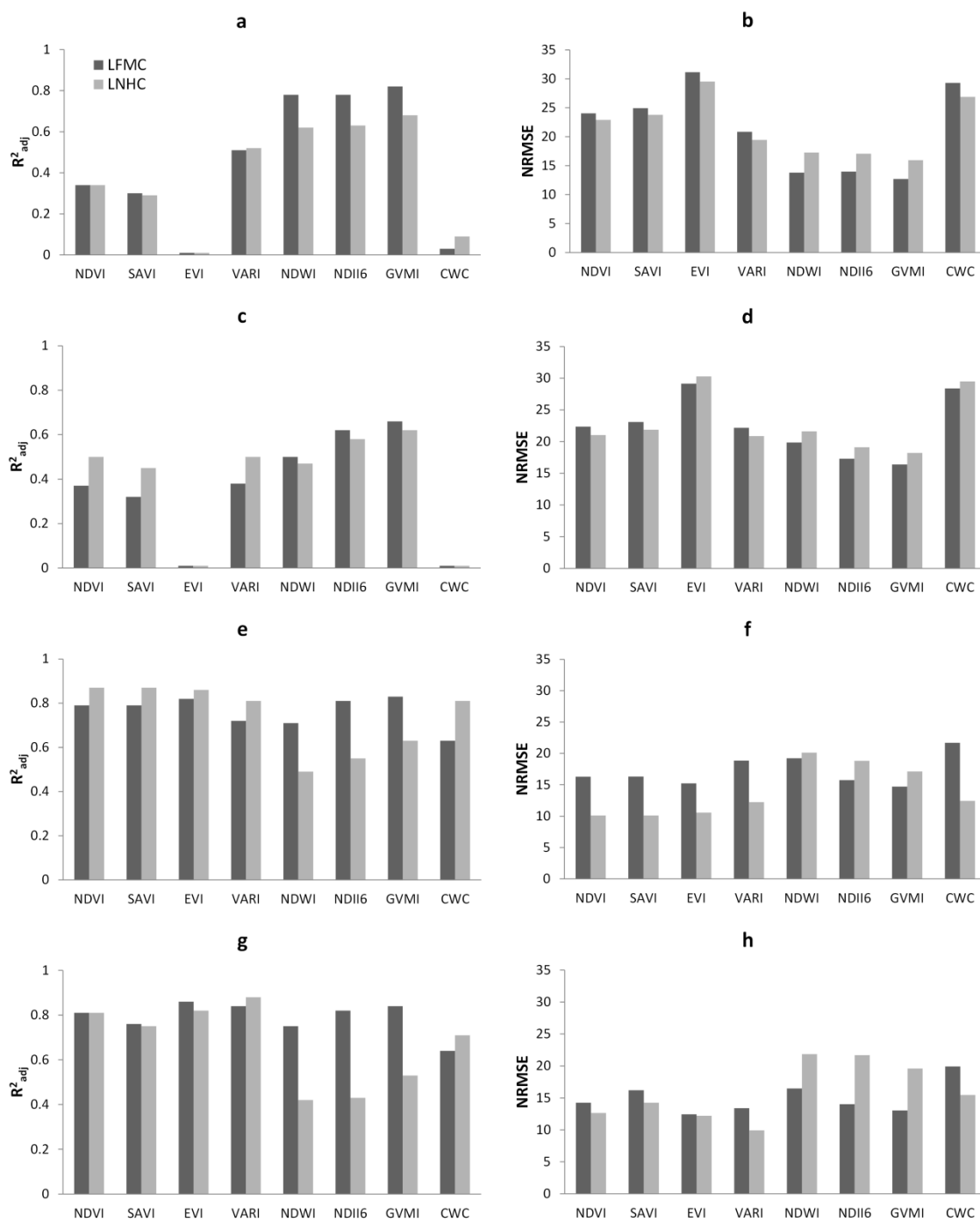
Figure 4.6 R^2_{adj} and NRMSE of linear models for leaf spectra. (a-b) Lodgepole pine site 1, (c-d) lodgepole pine site 2, (e-f) big sagebrush site 1, (g-h) big sagebrush site 2.
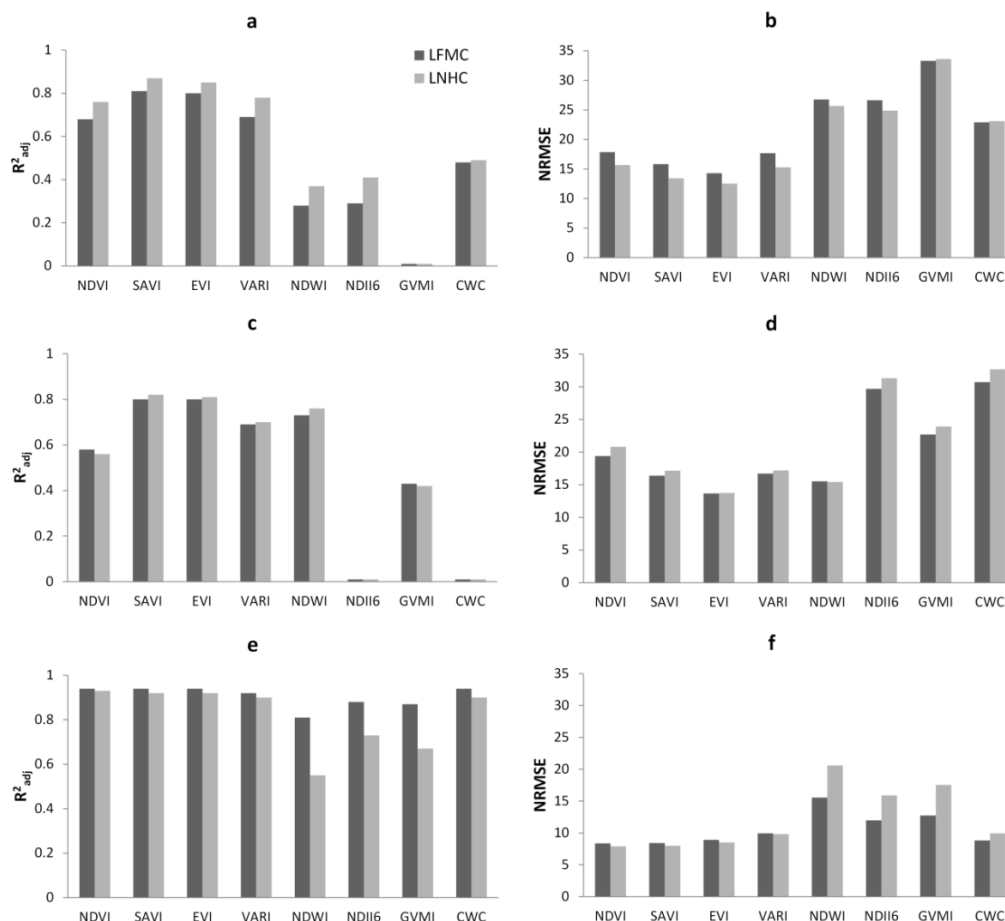
Figure 4.7 R^2_{adj} and NRMSE of linear models for MODIS spectra. (a-b) Lodgepole pine site 1, (c-d) lodgepole pine site 2, (e-f) big sagebrush site 1.

spectra. All greenness indices produced similar R^2_{adj} values about 0.92, while water indices produced slightly lower R^2_{adj} values. CWC of lodgepole pine produced lower R^2_{adj} values than greenness indices, while sagebrush's CWC showed comparable R^2_{adj} values. Comparison between LNHC and LFMC models showed similar NRMSE across all remote sensing variables for two species, with the largest difference of about 5% from water indices at sagebrush site 1.
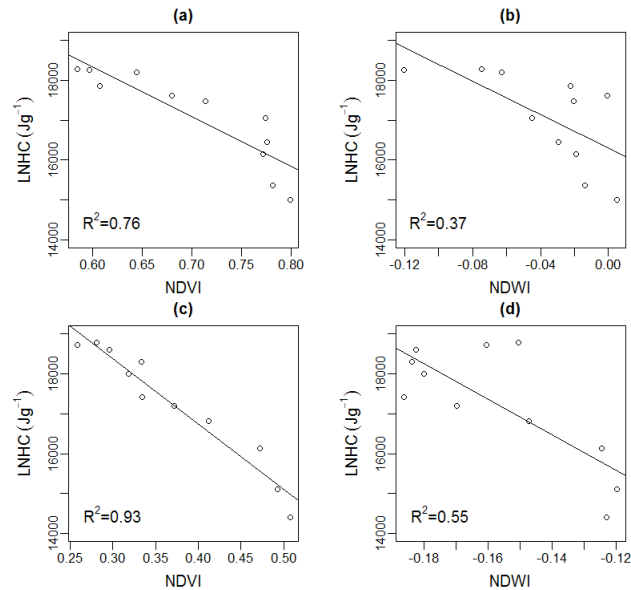
Figure 4.8 Linear correlation between LNHC and NDVI and NDWI in MODIS spectra. (a-b) Lodgepole pine site 1; (c-d) big sagebrush site 1.

4.4 Discussion

This study showed a species-dependent temporal trend in LFMC, HC and LNHC during the growth season. Lodgepole pine generally had larger LFMC/HC and smaller LNHC than big sagebrush at the same date. As LFMC decreased in lodgepole pine and big sagebrush, HC and LNHC increased by a different mechanism. Qi et al. (2014) demonstrated that a seasonal decrease in LFMC in lodgepole pine current-year growth needles was mainly attributed to dry matter increase, where LFMC decrease in sagebrush resulted from both water and dry matter in similar weight. Multiple biochemical components in the dry matter covaried during the season, causing interspecies HC difference between lodgepole pine and sagebrush. By considering the water heat sink, LNHC and LFMC had a negative, strongly correlated linear relationship. Lodgepole pine showed a LNHC about 1000 J g^{-1} higher than sagebrush at the same LFMC, meaning that

LFMC might be a less complete proxy of fire danger. This difference in LNHC was caused by HC difference between pine and sagebrush, which was likely due to different biochemical composition in the dry matter. The Rothermel (1972) model accounts for both LFMC and HC in the surface fire spread rate function. LFMC and HC were measured separately to represent specific fuel models, with HC assumed to be uniform across seasons and most fuel types on a per dry mass basis. I used standard HC values (18600 J g^{-1}, or 8000 BTU lb^{-1} in Abini 1976, Scott and Burgan 2005) to calculate standard net heat as function 4.3. The standard net heat consistently underestimated the LNHC for two species, and the estimation difference become larger with higher LNHC (Figure 4.9). LNHC provides a direct measure to aggregate these two variables for an appropriate proxy for fire danger. LNHC is easily measured in the calorimeter and can use the same samples as used for measuring LFMC, so it would be valuable to include LNHC in field sampling protocols along with LFMC.

My study also demonstrated that LNHC can be spectrally estimated with vegetation indices and RTM inversion with comparable correlations and error to LFMC. Indices based on water absorption features outperformed indices based on chlorophyll absorption and differences in visible-NIR reflectance at the leaf scale, likely since LNHC is more directly related to water absorption than chlorophyll absorption. The reversal in the performance of water absorption and greenness-based indices for MODIS data is potentially attributable to the multiple scattering effects in canopies. Linear regression models showed that vegetation indices can estimate LNHC and LFMC with comparable NRMSE and R^2_{adj} in MODIS pixel spectra. For example, EVI produced the highest R^2_{adj} values (0.8) and smallest NRMSE (13.7%) in both LFMC and LNHC models at two
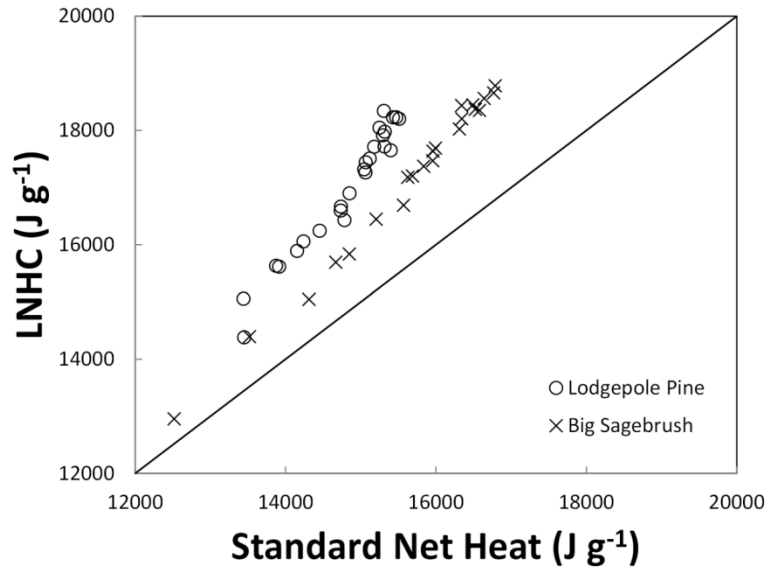
Figure 4.9 Comparison between LNHC and standard net heat. Standard net heat was calculated as standard HC subtracted by water heat sink as function 4.2.

lodgepole pine sites. Previous studies have shown that vegetation indices and RTM methods had comparable performance for estimating LFMC, but RTM was more robust for applications across different species and sites (Yebra et al. 2008). The RTM-inverted CWC generated different results between leaf spectra and MODIS pixel data. It showed similar performance as vegetation indices at sagebrush sites, but it did not produce high R^2_{adj} values at lodgepole pine sites. The spatial estimation of LNHC at MODIS scale could be incorporated into fire behavior models. Future work is needed to explore the upscaling of LNHC from leaf to canopy scale with RTM simulation.

4.5 Conclusions

This study introduced a new variable LNHC to facilitate fire danger assessment and fire behavior modeling. LNHC in lodgepole pine and sagebrush increased from July

to October as the LFMC decreased, and it showed a negative linear correlation LFMC. Two species produced different LHNC at the same LFMC due to different biochemical components in the leaf dry mass. This finding demonstrates the complexity of using LFMC as the fire danger indicator. LNHC is designed to measure actual heat release by considering both heat source by dry mass and heat sink by fuel moisture. It subtracts the HC of dry mass by absorbed heat for preheating and water evaporation. The LNHC could provide more direct measurement of energy release than LFMC. This study demonstrated the potential utility of using remote sensing variables to estimate LNHC. Greenness indices showed better modeling performance than water indices in MODIS spectra, though CWC did not produce better results over standard vegetation indices. LNHC could be estimated with similar NRMSE as LFMC. In combination with future analysis at canopy scale, this study showed the promising potential of remote sensing of LNHC to supplement assumption of constant HC in fuel models without having to separately model HC in addition to LMFC. Spatial and temporal monitoring of LNHC could be of great benefit to fire behavior modeling and fire danger estimation with the availability of models capable of appropriately using this information.

CHAPTER 5

CONCLUSIONS

This dissertation focused on the physical foundations of remote sensing estimation of LFMC and fire danger. Chapters 2-4 dealt with three perspectives of LFMC seasonal variation. All research questions were answered by this dissertation and research objectives were fulfilled.

The research questions in Chapter 2 were: "1) Whether soil moisture has potential as an LFMC proxy? 2) How does soil moisture as a proxy for LFMC estimation compare to remote sensing proxies?" Chapter 2 collected ground soil moisture measurements and MODIS data in 2010 and 2011 for Gambel oak (*Quercus gambelii* Nutt) and big sagebrush (*Artemisia tridentata* Nutt), and constructed linear regression models with field-sampled LFMC. The results demonstrated that soil moisture can produce the lowest mean absolute error (MAE) in predicted LFMC values at most of the sites when compared with remote sensing measures. Soil moisture can potentially provide an alternative to remote sensing for frequent temporal monitoring for LFMC estimation. When sites were pooled, canopy water content (CWC) had stronger correlations with LFMC than normalized difference vegetation index (NDVI) or normalized difference water index (NDWI). Although remote sensing proxies showed less strong correlations with LFMC in this study, their estimation power could be improved by using high quality

MODIS data and more homogeneous sites. MAE values for all proxies were frequently above 20 % LFM at individual sites. Despite this relatively large error, remote sensing and soil moisture data may still be useful for improving the understanding of spatial and temporal trends in LFMC.

The research questions in Chapter 3 were: "1) How do LFMC and dry mass change during the growth season? 2) How do biochemical components in dry mass contribute to LFMC change and covary over time? 3) How can leaf spectroscopy track seasonal variability in LFMC and dry mass? 4) Can PLSR provide new insights into temporal spectral variation due to changes in LFMC and dry mass?" Chapter 3 integrated 5 months of field sample and lab measurements in May-October 2012 for two species common in the western US, lodgepole pine (*Pinus contorta* Douglas ex Loudon) and big sagebrush (*Artemisia tridentata* Nutt), and then examined seasonal variation in LFMC, leaf dry mass, and leaf spectroscopy. The results showed that new lodgepole pine needles initially had higher LFMC and a smaller proportion of dry mass, but differences between new and old needles converged as the new needles matured. New needle dry mass had strong temporal trends, and dry mass explained more variation in LFMC than water in both new and old needles. Sagebrush leaves exhibited decreasing trends in LFMC, but water and dry mass comparably contributed to LFMC seasonal variation. Spectroscopic analysis using partial least squares regression (PLSR) showed good modeling accuracy for LFMC temporal variation in new needles ($R^2 = 0.94$, RMSE = 5.84%), old needles ($R^2 = 0.72$, RMSE = 3.51%), and sagebrush ($R^2 = 0.91$, RMSE = 21.03%). Spectral variation in response to changing LFMC and dry mass was difficult to isolate from broader spectral trends due to chlorophyll absorption, leaf structure, water absorption,

and covaried biochemical components. The results stressed cautious spectral interpretation and wavelength selection for LFMC estimation in some species (e.g., lodgepole pine), since temporal changes in spectra may dominantly reflect temporal variation in dry mass, pigments, and/or structure rather than water content. Since new needles should have stronger spectral expression at the canopy scale, differing temporal trends in new and old lodgepole pine needles provide an additional complicating factor for remote monitoring of LFMC.

The research questions in Chapter 4 were: "1) How do LFMC and leaf net heat content (LNHC) change over time; 2) What is the relationship between LFMC and LNHC; 3) Is it possible to remotely estimate LNHC?" The study measured LNHC and LFMC for lodgepole pine and big sagebrush in July-October, 2012. I also collected leaf-scale spectroscopy and MODIS pixel spectra over the same sampling period. Lab spectra of leaf samples convolved to MODIS bands and single MODIS pixel spectra were used to calculate vegetation indices. Linear regression was used to compare relationships between vegetation indices and both LNHC and LFMC over time. The results showed LNHC and LFMC were strongly correlated for current-year needles and sagebrush leaves, with LNHC increasing over time and LFMC decreasing over time. Relationships between LNHC and LFMC were species dependent. Vegetation indices of MODIS pixel spectra generally produced comparable R-squared values and normalized root mean squared error for fits to LNHC and LFMC trends. Greenness indices were more strongly correlated with LNHC than water indices. This study suggests that LNHC is a more direct measurement of fire danger than LFMC. MODIS data have potential utility for estimating temporal trends in LNHC.

LFMC is one of the primary fuel variables in fire danger assessment systems (e.g., Deeming et al. 1978; Stocks et al. 1989) and fire behavior models (e.g., Andrews 1986; Rothermel 1972). LFMC changes with two fundamental mechanisms, environmental conditions and plant physiological processes. The accurate LFMC prediction requires a deeper understanding of LFMC seasonal changes with these two mechanisms. The first major contribution of this dissertation is advancing current knowledge of how LFMC varies with soil moisture as one environmental variable. It constructs empirical relationships between soil moisture and LFMC of Gambel oak and big sagebrush. The decreasing trend in the soil moisture correlates with the dry-down trend in LFMC during the dry and hot summer and fall. This demonstrates that soil water availability is likely a control on LFMC. The second contribution is decoupling the water and dry matter sources of LFMC seasonal change by focusing on lodgepole pine and sagebrush. For the first time, I examine biochemical components varying along with LFMC and explain the role of dry matter. This result warns against the false assumption of constant dry matter and suggests a more careful interpretation of LFMC decrease as a dry-down signal.

The third contribution is to the remote sensing estimation of LFMC. To date, no satellite-based LFMC product has been operationally integrated into wildfire danger assessment. One of the theoretical challenges is the difficult retrieval of dry matter. The absorption feature of water content usually masks the dry matter spectral signature, since water has larger absorption coefficients over most of the solar-reflected spectrum. Some physical methods for estimating LFMC have relied on the assumption of constant dry matter during the season (Riaño et al. 2005). As the first study emphasizing the temporal trend in dry matter, this study demonstrates the dry matter change over time, and the

spectral response to LFMC and dry matter change is not isolated from confounding absorptions of water, pigment and biochemical components. This study will potentially improve the physical methods by providing realistic ranges of parameters for solving the ill-posed RTM inversion problem. This study will also enhance the utility of PLSR in imaging spectroscopy for LFMC estimation. The fourth contribution is improving on LFMC by introducing LNHC as a direct measure of fire risk. This study demonstrates the potential for LNHC estimation with remotely sensed data such as MODIS. The spatially variable LNHC will allow a more comprehensive fire risk assessment system and could be used by fire behavior modeling.

Operational LFMC or LNHC estimation with remote sensing is important for spatial and temporal monitoring of fire danger. Future work will need to increase prediction accuracy. Hyperspectral sensors such as AVIRIS and the planned HyspIRI mission would provide continuous spectral domain and higher spatial resolution to improve LFMC estimation, though their temporal resolution cannot provide frequent monitoring capacity. Moderate resolution sensors such as MODIS and newly launched VIIRS would potentially provide weekly or daily products by validation with hyperspectral sensors. This dissertation conducted spectroscopic analysis at leaf scale. Future studies will examine changes in canopy spectra in response to LFMC and dry matter over time, by either continuous field spectroscopy over canopy or satellite data in homogeneous species patch. More research is needed to test how covaried biochemical components are expressed in spectra at canopy scale, and for evergreen plants, how canopy spectra resemble combinations of spectral characteristics from new and old leaves. This research calls for a more careful interpretation by the end-user community for

LFMC seasonal variation in conifer species, since LFMC decrease coincides with dry matter accumulation and LNHC increase. This research will contribute to the fundamental knowledge of the risk and impact of wildfires. It will also provide significant societal benefit for the fire management community and governmental agencies, assisting in development of strategies and policies for disaster and resource management.

APPENDIX

LEAF SPECTROSCOPY PROCEDURES

This study used field spectrometer ASD FieldSpec4 High-Res spectrometer linked with an ASD integrating sphere (model RTS-3ZCR2) to measure needle reflectance and transmittance. Smaller than broad-leaves, needles cannot cover the whole sample port on the integrating sphere. Two categories of methods have been developed to handle needles and small leaves: Daughtry's method (Daughtry et al. 1989) revised from Mesarch (Mesarch et al. 1999), and Harron's method (Harron 2000). In Daughtry's method, needles were laid side by side to form a flat mat. Optical properties were measured on the mat, and individual needles reflectance and transmittance were derived from the mat measurements by correcting gap fraction between needles. Mesarch investigated the effect of gap fraction on optical measurements and proposed a threshold of 0.2 under which the measurements could be trusted. He also suggested an image analysis-based method for calculating gap fraction to replace error-prone painting methods in Daughtry's paper. The gap fraction has been the major criticism in Daughtry's method. It significantly changes the optical measurements by introducing complex light scattering between gaps, mostly due to the hemicylindrical shape of needles. As a result, it decreases the signal-to-noise ratio especially in longer wavelengths. To solve this problem, Harron's method designed a customized needle-carrier to hold the samples, which fixed the gap fraction and eliminated specular reflectance on the abaxial surface. Mathematic calculation can correct the carrier effect and derive individual needle reflectance and transmittance.

In my study, I choose the Daughtry's method instead of Harron's method. One reason is the timely schedule and lack of access to the manufacture of leaf sample holders. More importantly, Harron's thesis showed that the almost constant offset between

measurements in Daughtry's method and Harron's method was majorly attributed to underestimated gap fraction when measuring abaxial surface, where curved surfaces enlarged the actual gaps between needles by specular reflection. The geometrical design of needle carrier caused an underestimation of needle reflectance and transmittance (Zhang et al. 2008). It is thus reasonable to argue that better work on the needle mat configuration and gap fraction computation would limit the errors in optical measurements.

The function to calculate reflectance is (Mesarch et al. 1999):

$$\rho = \frac{\rho_{total}}{1 - GF} \tag{1}$$

where ρ = reflectance of individual needle

$$\rho_{total} = \frac{R_{total} - STR}{REF - STR} \tag{2}$$

R_{total} = total reflected radiation from the sample

STR = tray light radiation

REF = reflected radiation from a BaSO4 reference standard

GF = gap fraction on the sample

The function to calculate transmittance is:

$$\tau = [\tau_{total} - (\rho_w GF)]\frac{1}{1 - GF} \tag{3}$$

τ = transmittance through individual needle

$$\tau_{total} = \frac{T_{total}}{REF - STR} \tag{4}$$

T_{total} = total transmitted radiation through the sample

ρ_w = reflectance of the integrating sphere wall

Different port configuration on the integrating sphere needs to be applied to the

measurements above. Turn on the spectrometer at least 15 min to warm up before taking measurements. Collecting all spectra in ratio mode (i.e., run a white reference with the sphere in the reflectance configuration) is preferred over collecting raw DN or radiance mode. Optimize the spectrometer and take the white reference first in each sample measurement. Reflectance port setup shown in Table A.1. Transmittance port setup shown in Table A.2. In equation (2), $\rho_{total} = \frac{(R_s - R_d) * R_r}{(1 - R_d)}$, where Rr = reflectance of the calibrated reference standard. In equation (4), $\tau_{total} = \frac{(T_s - R_d)}{(1 - R_d)}$.

Table A.1. Integrating sphere plug configuration in reflectance mode.

Port	Reflectance Reference	Reflectance Sample	Dark Reading (Stray light correction)
	Rr	Rs	Rd
[A]	Collimated light source	Collimated light source	Collimated light source
[B]	Sample+Light trap	Reference standard	Reference standard
[C]	Reference standard	Sample+Light trap	Open port with light trap
[D]	White plug	White plug	White plug
[E]	White plug	White plug	White plug

Table A.2. Integrating sphere plug configuration in transmittance mode.

Port	Reflectance Reference	Transmittance Sample	Dark Reading (Stray light correction)
	Rr	Ts	Rd
[A]	White plug	White plug	White plug
[B]	Uncalibrated zenith standard	Uncalibrated zenith standard	Open port with light trap
[C]	Sample	Open port with light trap	Uncalibrated zenith standard
[D]	Collimated light source	Collimated light source and sample	Collimated light source
[E]	White plug	White plug	White plug

Middleton et al. (1997) reported a clear discrepancy between needle adaxial and abaxial optical properties. To make more realistic estimation of needle albedo for upscaling to canopy level, I will measure both sides of needle surfaces. The average of abaxial and adaxial reflectance and transmittance will represent needle optical properties *in situ*. Ideally the needle should be arranged side by side at the same surface as closely as possible to make a relative homogenous flat mat. The needles are taped at two ends. I have designed a sample holder for needle and sagebrush leaves with an alignment mark with the purpose of :1) stabilize the bundle to minimize gap variation due to sample movement and gravity; 2) ensure the same needle area will fill the field of view of light source when changing ports configuration; 3) make the gap fraction measurement easier. Sagebrush leaves are too short to fit the sample port on the integrating sphere. The blue print of leaf mounts will be designed to align with ports on the integrating sphere in order to ensure the same area will be illuminated when changing plug configuration (Figure A.1). The sample holder painted in black does not contribute to the total reflectance or transmittance.
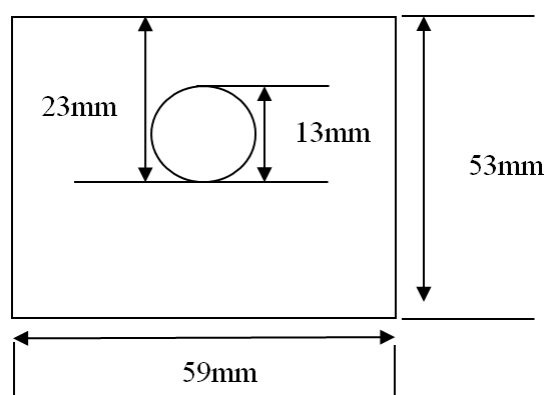
Figure A.1 Blue print of the sample holder.

The needle sample is subsequently scanned with a double-lamp desktop scanner at resolution of 1200 dpi above (to prevent the occurrence of needle objects shadow in scanned image). GF is retrieved from 8-bite gray-scale scanned images as the ratio of the total number of white pixels (air gaps, greater than a threshold value determined *in situ*, zero is black, 255 is white) to the number of pixels of the total measured (illuminated area) within the mount aperture (Di Vittorio 2009; Rautiainen et al. 2012). The spectroscopy steps are as follows:

1. For each one sample, 10-12 needles can make a flat needle mat on the sample holder (flat black painting cardboard). Clean the needle surfaces if needed. Put double-side tape on the holder sides first, be careful to align adaxial (flat) surfaces of needles on the holder and minimize the gap, cover two ends of needles with black PVC tape. Three to four sagebrush leaves can fill up the sample holder aperture. Try to align the leaf surface at the center of the aperture and gaps to the edge in order to minimize gap effect within the illumination area.

2. Group 16 samples into new and old categories. Set up spectrometer and integrating sphere and take lab spectroscopy separately. Connect the optical fiber to the top port of integrating sphere. Be careful to keep the fiber in a relaxed position. The underlying reason is that, assuming the variation within one category is less than 20%, the white reference measurement can be taken only once for each category, which will speed up following measurements.

3. In the new needle category, turn on the spectrometer 60 min before taking measurement, then the laptop. Turn on the light source 5 min before measurement. In RS3 software, "control" – "adjust configuration," increase the

"spectrum" to 200 in order to optimize the signal-to-noise ratio, especially in the SWIR2 (This means the spectrometer will take 200 scans and average them to one measurement).

Face the adaxial surface toward the sample port on the integrating sphere port [B]. Set up the integrating sphere in reference mode (R_r in Table A.1), optimize the spectrometer and take the white reference.

4. Take the stray light measurement (R_d in Table A.1). Only one measurement is necessary, and the measurement can be used repeatedly in future reflectance measurements.

5. Take one measurement of sample reflectance (R_s in Table A.1). This is the reflectance on adaxial surface. Repeat this step for all eight samples in one category.

6. Flip the sample to face abaxial surface toward sample port on the integrating sphere port [B]. Set up the integrating sphere in reference mode (R_r in Table A.1), optimize the spectrometer and take the white reference again.

7. Take the stray light measurement (R_d in Table A.1). Only one measurement is necessary, and the measurement can be used repeatedly in future reflectance measurements.

8. Take one measurement of sample reflectance (R_s in Table A.1). This is the reflectance on abaxial surface. Repeat this step for all eight samples in one category.

9. Face the adaxial surface toward the light source on the integrating sphere port [C]. Replug the integrating sphere in transmittance mode (R_r in Table A.2),

optimize the spectrometer and take the white reference.

10. Take the spray light (R_d in Table A.2). Only one measurement is necessary, and the measurement can be used repeatedly in future transmittance measurements.

11. Take one measurement of sample transmittance (T_s in Table A.2). This is the transmittance on adaxial surface. Repeat this step for all eight samples in one category.

12. Flip the sample to face abaxial surface toward the light source on the integrating sphere port [C]. Replug the integrating sphere in transmittance mode (R_r in Table A.2), optimize the spectrometer and take the white reference again.

13. Take the spray light (R_d in Table A.2). Only one measurement is necessary, and the measurement can be used repeatedly in future transmittance measurements.

14. Take one measurement of sample transmittance (T_s in Table A.2). This is the transmittance on abaxial surface. Repeat this step for all eight samples in one category.

Based on the statement in step 2, repeat steps 3-14 for old needle category.

REFERENCES

Albini, F.A., 1976, Estimating wildfire behavior and effects, Gen. Tech. Rep. INT-30, Ogden, Utah: Department of Agriculture, Forest Service, Intermountain Forest and Range Experiment Station, 92 p.

Andrews, P.L., 1986, BEHAVE: Fire behavior prediction and fuel modeling Subsystem-BURN Subsystem, Part 1, Gen. Tech. Rep. INT-194, In U.F. Services (Ed.), Ogden, UT.

Andrews, P.L., Bevins, C.D., and Seli, R.C., 2003, BehavePlus fire modeling system, version 2.0: User's Guide, Gen. Tech. Rep. RMRS-GTR-106WWW, Ogden, UT: Department of Agriculture, Forest Service, Rocky Mountain Research Station, 132 p.

Asner, G., and Martin, R., 2008, Spectral and chemical analysis of tropical forests: Scaling from leaf to canopy levels, Remote Sensing of Environment, 112, 3958-3970.

Asner, G.P., Martin, R.E., Tupayachi, R., Emerson, R., Martinez, P., Sinca, F., Powell, G.V.N., Wright, S.J., and Lugo, A.E., 2011, Taxonomy and remote sensing of leaf mass per area (LMA) in humid tropical forests, Ecological Applications, 21, 85-98.

Bansal, S., and Germino, M.J., 2009, Temporal variation of nonstructural carbohydrates in montane conifers: Similarities and differences among developmental stages, species and environmental conditions, Tree Physiology, 29, 559-568.

Barrs, H., and Weatherley, P., 1962, A re-examination of the relative turgidity technique for estimating water deficits in leaves, Australian Journal of Biological Sciences, 15, 413-428.

Bessie, W.C., and Johnson, E.A., 1995, The relative importance of fuels and weather on fire behavior in subalpine forests, Ecology, 76: 747-762.

Bowman, D.M.J.S., Balch, J.K., Artaxo, P., Bond, W.J., Carlson, J.M., Cochrane, M.A., D'Antonio, C.M., DeFries, R.S., Doyle, J.C., Harrison, S.P., Johnston, F.H., Keeley, J.E., Krawchuk, M.A., Kull, C.A., Marston, J.B., Moritz, M.A., Prentice, I.C., Roos, C.I., Scott, A.C,. Swetnam, T.W., Van Der Werf, G.R., and Pyne, S.J.,

2009, Fire in the earth system, Science, 324, 481-484.

Bowyer, P., and Danson, F., 2004, Sensitivity of spectral reflectance to variation in live fuel moisture content at leaf and canopy level, Remote Sensing of Environment, 92, 297-308.

Brocca, L., Morbidelli, R., Melone, F., and Moramarco, T., 2007, Soil moisture spatial variability in experimental areas of central Italy, Journal of Hydrology, 333, 356-373.

Burgan, R.E. and Rothermel, R. C, 1984, BEHAVE: Fire behavior prediction and fuel modeling system – FUEL subsystem, Gen. Tech. Rep. INT-167, Ogden, UT: US Department of Agriculture, Forest Service, Intermountain Forest and Range Experiment Station, 126 p.

Burgan, R.E., Klaver, R.W., and Klaver, J.M., 1998, Fuel models and fire potential from satellite and surface observations, International Journal of Wildland Fire, 8, 159-170.

Caccamo, G., Chisholm, L.A., Bradstock, R.A., Puotinen, M.L., and Pippen, B.G., 2012 Monitoring live fuel moisture content of heathland, shrubland and sclerophyll forest in south-eastern Australia using MODIS data, International Journal of Wildland Fire, 21, 257-269.

Ceccato, P., Flasse, S.P., Tarantola, S., Jacquemoud, S.P., and Gre´goire, J.-M., 2001, Detecting vegetation leaf water content using reflectance in the optical domain, Remote Sensing of Environment, 77, 22-33.

Ceccato, P., Gobron, N., Flasse, S.P., Pinty, B., and Tarantola, S., 2002, Designing a spectral index to estimate vegetation water content from remote sensing data: Part 1 theoretical approach, Remote Sensing of Environment, 82, 188-197.

Cheng, T., Rivard, B., and Sánchez-Azofeifa, A., 2011, Spectroscopic determination of leaf water content using continuous wavelet analysis, Remote Sensing of Environment, 115, 659-670.

Cheng, T., Rivard, B., Sánchez-Azofeifa, A.G., Féret, J.-B., Jacquemoud, S., and Ustin, S.L, 2014, Deriving leaf mass per area (LMA) from foliar reflectance across a variety of plant species using continuous wavelet analysis, ISPRS Journal of Photogrammetry and Remote Sensing, 87, 28-38.

Chuvieco, E., Aguado, I., Cocero, D., and Riano, D., 2003, Design of an empirical index to estimate fuel moisture content from NOAA-AVHRR images in forest fire danger studies, International Journal of Remote Sensing, 24, 1621-1637.

Chuvieco, E., Cocero, D., Riaño, D., Martin, P., Martínez-Vega, J., De La Riva, J., and

Pérez, F., 2004, Combining NDVI and surface temperature for the estimation of live fuel moisture content in forest fire danger rating, Remote Sensing of Environment 92: 322-331.

Chuvieco, E., González, I., Verdú, F., Aguado, I., and Yebra, M., 2009, Prediction of fire occurrence from live fuel moisture content measurements in a Mediterranean ecosystem, International Journal of Wildland Fire, 18, 430-441.

Chuvieco, E., Riaño, D., Aguado, I., and Cocero, D., 2002, Estimation of fuel moisture content from multitemporal analysis of Landsat Thematic Mapper reflectance data: Applications in fire danger assessment, International Journal of Remote Sensing, 23, 2145-2162.

Chuvieco, E., Wagtendonk, J., Riaño, D., Yebra, M., and Ustin, S. L., 2009, Estimation of fuel conditions for fire danger assessment, Pages 83-96 in: Chuvieco, E., editor, Earth observation of wildland fires in Mediterranean ecosystems, Springer, New York, USA.

Cochrane, M.A., 2003, Fire science for rainforests, Nature, 421, 913-919.

Colombo, R., Meroni, M., Marchesi, A., Busetto, L., Rossini, M., Giardino, C., and Panigada, C., 2008, Estimation of leaf and canopy water content in poplar plantations by means of hyperspectral indices and inverse modeling, Remote Sensing of Environment, 112, 1820-1834.

Curran, P.J., 1989, Remote sensing of foliar chemistry, Remote Sensing of Environment, 30, 271-278.

Curran, P.J., Dungan, J.L., Macler, B.A., Plummer, S.E., and Peterson, D.L., 1992, Reflectance spectroscopy of fresh whole leaves for the estimation of chemical concentration, Remote Sensing of Environment, 39, 153-166.

Danson, F., and Bowyer, P., 2004, Estimating live fuel moisture content from remotely sensed reflectance, Remote Sensing of Environment, 92, 309-321.

Datt, B., 1999, Remote sensing of water content in eucalyptus leaves, Australian Journal of Botany, 47, 909-923.

Daughtry, C.S.T., Biehl, L.L., and Ranson, K.J., 1989, A new technique to measure the spectral properties of conifer needles, Remote Sensing of Environment, 27, 81-91.

Dawson, T.P., Curran, P.J., and Plummer, S.E., 1998, The biochemical decomposition of slash pine needles from reflectance spectra using neural networks, International Journal of Remote Sensing, 19, 1433-1438.

Deeming, J.E., Burgan, R.E., and Cohen, J.D., 1978, The national fire-danger rating

system -1978, USDA Forest Service General Technical Report INT-39, Intermountain Forest and Range Experiment Station, Ogden, UT, USA.

Demarez, V., Gastellu-Etchegorry, J.P., Mougin, E., Marty, G., Proisy, C., Dufrêne, E., and Dantec, V.L., 1999, Seasonal variation of leaf chlorophyll content of a temperate forest, Inversion of the PROSPECT model, International Journal of Remote Sensing, 20, 879-894.

Dennison, P.E., and Moritz, M.A., 2009, Critical live fuel moisture in chaparral ecosystems: A threshold for fire activity and its relationship to antecedent precipitation, International Journal of Wildland Fire, 18, 1021-1027.

Dennison, P.E., Moritz, M.A., and Taylor, R.S., 2008, Evaluating predictive models of critical live fuel moisture in the Santa Monica Mountains, California, International Journal of Wildland Fire, 17, 18-27.

Dennison, P.E., Roberts, D.A., Peterson, S.H., and Rechel, J., 2005, Use of normalized difference water index for monitoring live fuel moisture, International Journal of Remote Sensing, 26, 1035-1042.

Dennison, P.E., Roberts, D.A., Thorgusen, S.R., Regelbrugge, J.C., Weise, D., and Lee, C., 2003, Modeling seasonal changes in live fuel moisture and equivalent water thickness using a cumulative water balance index, Remote Sensing of Environment, 88, 442-452.

Dibble, A.C., White, R.H., and Lebow, P.K., 2007, Combustion characteristics of north-eastern USA vegetation tested in the cone calorimeter: Invasive versus non-invasive plants, International Journal of Wildland Fire, 16, 426-443.

Dimitrakopoulos, A.P., and Bemmerzouk, A.M., 2003, Predicting live herbaceous moisture content from a seasonal drought index, International Journal of Biometeorology, 47, 73-79.

Dimitrakopoulos, A.P., and Panov, P.I., 2001, Pyric properties of some dominant Mediterranean vegetation species, International Journal of Wildland Fire, 10, 23-27.

Di Vittorio, A.V., 2009, Enhancing a leaf radiative transfer model to estimate concentrations and in vivo specific absorption coefficients of total carotenoids and chlorophylls a and b from single-needle reflectance and transmittance, Remote Sensing of Environment, 113, 1948-1966.

Doughty, C., Asner, G., and Martin, R., 2011, Predicting tropical plant physiology from leaf and canopy spectroscopy, Oecologia, 165, 289-299.

Elvidge, C.D., 1990, Visible and near infrared reflectance characteristics of dry plant

materials, International Journal of Remote Sensing, 11, 1775-1795.

Entin, J.K., Robock, A., Vinnikov, K.Y., Hollinger, S.E., Liu, S., and Namkai, A., 2000, Temporal and spatial scales of observed soil moisture variations in the extratropics, Journal of Geophysical Research, 105, 865-877.

FAO, 2001, Global forest fire assessment 1990 - 2000, Forest Resources Assessment Working Paper, Rome, Italy.

Fensholt, R., Sandholt, I., Proud, S.R., Stisen, S., and Rasmussen, M.O., 2010, Assessment of MODIS sun-sensor geometry variations effect on observed NDVI using MSG SEVIRI geostationary data, International Journal of Remote Sensing, 31, 6163-6187.

Féret, J.-B., François, C., Gitelson, A., Asner, G.P., Barry, K.M., Panigada, C., Richardson, A.D., and Jacquemoud, S., 2011, Optimizing spectral indices and chemometric analysis of leaf chemical properties using radiative transfer modeling, Remote Sensing of Environment, 115, 2742-2750.

Finney, M.A., 1998, FARSITE: Fire area simulator-model development and evaluation, Res. Pap. RMRSRP-4, Fort Collins, CO: US Department of Agriculture, Forest Service, Rocky Mountain Research Station, 47 p.

Fourty, T., and Baret, F., 1997, Vegetation water and dry matter contents estimated from top-of-the-atmosphere reflectance data: A simulation study, Remote Sensing of Environment, 61, 34-45.

Fourty, T., Baret, F., Jacquemoud, S., Schmuck, G., and Verdebout, J., 1996, Leaf optical properties with explicit description of its biochemical composition: Direct and inverse problems, Remote Sensing of Environment, 56, 104-117.

Gao, B.-C., 1996, NDWI-A normalized difference water index for remote sensing of vegetation liquid water from space, Remote Sensing of Environment 58: 257-266.

Gao, B.-C., and Goetz, A.F.H., 1995, Retrieval of equivalent water thickness and information related to biochemical components of vegetation canopies from AVIRIS data, Remote Sensing of Environment, 52, 155-162.

García, M., Chuvieco, E., Nieto, H., and Aguado, I., 2008, Combining AVHRR and meteorological data for estimating live fuel moisture content, Remote Sensing of Environment, 112, 3618-3627.

Gitelson, A.A., Kaufman, Y.J., Stark, R., and Rundquist, D., 2002, Novel algorithms for remote estimation of vegetation fraction, Remote Sensing of Environment, 80, 76-87.

Gond, V., De Pury, D.G.G., Veroustraete, F., and Ceulemans, R., 1999, Seasonal variations in leaf area index, leaf chlorophyll, and water content: Scaling-up to estimate fAPAR and carbon balance in a multilayer, multispecies temperate forest, Tree Physiology, 19, 673-679.

Hardisky, M.A., Klemas, V., and Smart, R.M., 1983, The influence of soil salinity, growth form, and leaf moisture on the spectral radiance of Spartina alterniflora canopies, Photogrammetric Engineering & Remote Sensing, 49, 77-83.

Harron, J., 2000, Optical properties of phytoelements in conifers. York University.

Horler, D.N.H., Dockray, M., and Barber, J., 1983, The red edge of plant leaf reflectance, International Journal of Remote Sensing, 4, 273-288.

Huete, A., Didan, K., Miura, T., Rodriguez, E.P., Gao, X., and Ferreira, L.G., 2002, Overview of the radiometric and biophysical performance of the MODIS vegetation indices, Remote Sensing of Environment, 83, 195-213.

Huete, A.R., 1988, A soil-adjusted vegetation index (SAVI), Remote Sensing of Environment, 25, 295-309

Jacquemoud, S., Baret, F., Andrieu, B., Danson, F.M., and Jaggard, K., 1995, Extraction of vegetation biophysical parameters by inversion of the PROSPECT+SAIL models on sugar beet canopy reflectance data: Application to TM and AVIRIS sensors, Remote Sensing of Environment, 52, 163-172.

Jolly W.M., Hadlow, A.M., and Huguet, K., 2014, Decoupling seasonal changes in water content and dry matter to predict live conifer foliar moisture content, International Journal of Wildland Fire, 23, 480-489. .

Jurdao, S., Yebra, M., Guerschman, J.P., and Chuvieco, E., 2013, Regional estimation of woodland moisture content by inverting radiative transfer models, Remote Sensing of Environment, 132, 59-70.

Keetch, J.J., and Byram, G.M., 1968, A drought index for forest fire control, USDA Forest Service Research Paper SE-38, Southeastern Forest Experiment Station, Asheville, NC, USA.

Kolb, J,K., and Sperry, J.S., 1999, Differences in drought adaptation between subspecies of sagebrush (Artemisia tridentata), Ecology, 80, 2373-2384.

Kokaly, R.F., and Clark, R.N., 1999, Spectroscopic determination of leaf biochemistry using band-depth analysis of absorption features and stepwise multiple linear regression, Remote Sensing of Environment, 67, 267-287.

Kozlowski, T.T., 1964, Shoot growth in woody plants, The Botanical Review, 30, 335-

392.

Kozlowski, T.T., and Clausen, J.J., 1965, Changes in moisture contents and dry weights of buds and leaves of forest trees, Botanical Gazette, 126, 20-26.

Kramer, P.J., and Kozlowski, T.T., 1960, Physiology of trees, New York: McGraw Hill Book Co.

Kuusk, A., 1995, A fast invertible canopy reflectance model, Remote Sensing of Environment, 51, 342-350.

Lawson, B.D., and Hawkes, B.C., 1989, Field evaluation of moisture content model for medium sized logging slash, Pages 247-257 in: Proceedings of the 10th Conference on Fire and Forest Meteorology, Ottawa, Canada.

le Maire, G., François, C., Soudani, K., Berveiller, D., Pontailler, J.-Y., Bréda, N., Genet, H., Davi, H., and Dufrêne, E., 2008, Calibration and validation of hyperspectral indices for the estimation of broadleaved forest leaf chlorophyll content, leaf mass per area, leaf area index and leaf canopy biomass, Remote Sensing of Environment, 112, 3846-3864.

Li, L., Ustin, S.L., and Riaño, D., 2007, Retrieval of fresh leaf fuel moisture content using Genetic Algorithm Partial Least Squares (GA-PLS) modeling, IEEE Geoscience and Remote Sensing Letters, 4, 216-220.

Littell, J.S., McKenzie, D., Peterson, D.L., and Westerling, A.L., 2009, Climate and wildfire area burned in western US ecoprovinces, 1916-2003, Ecological Applications, 19, 1003-1021.

Maki, M., Ishiahra, M., and Tamura, M., 2004, Estimation of leaf water status to monitor the risk of forest fires by using remotely sensed data, Remote Sensing of Environment, 90, 441-450.

Martens, H., and Naes, T., 2001, Multivariate calibration by data compression, In W. Norris, & K. Norris (Eds.), near-infrared technology in the agriculture and food industries (pp. 59-100). St. Paul, Minnesota, USA: American Association of Cereal Chemists.

McKenzie, D., Gedalof, Z., Peterson, D.L., and Mote, P., 2004, Climatic change, wildfire, and conservation, Conservation Biology, 18, 890-902.

Mediavilla, S., González-Zurdo, P., García-Ciudad, A., and Escudero, A., 2011, Morphological and chemical leaf composition of Mediterranean evergreen tree species according to leaf age, Trees - Structure and Function, 25, 669-677.

Mesarch, M.A., Walter-Shea, E.A., Asner, G.P., Middleton, E.M., and Chan, S.S., 1999,

A revised measurement methodology for conifer needles spectral optical properties: Evaluating the influence of gaps between elements, Remote Sensing of Environment, 68, 177-192.

Middleton, E.M., Chan, S.S., Rusin, R.J., and Mitchell, S.K., 1997, Optical properties of black spruce and jack pine needles at BOREAS sites in Saskatchewan, Canada, Canadian Journal of Remote Sensing, 23, 108-119.

Miller, J.R., Wu, J., Boyer, M.G., Belanger, M., and Hare, E.W., 1991, Seasonal patterns in leaf reflectance red-edge characteristics, International Journal of Remote Sensing, 12, 1509-1523.

Peñuelas, J., and Filella, L., 1998, Technical focus: Visible and near-infrared reflectance techniques for diagnosing plant physiological status, Trends in Plant Science, 3, 151-156.

Peñuelas, J., Piñol, J., Ogaya, R., and Filella, I., 1997, Estimation of plant water concentration by the reflectance Water Index WI (R900/R970), International Journal of Remote Sensing, 18, 2869-2875.

Peterson, S.H., Roberts, D.A., and Dennison, P.E., 2008, Mapping live fuel moisture with MODIS data: A multiple regression approach, Remote Sensing of Environment, 112, 4272-4284.

Plucinski, M.P., Anderson, W.R., Bradstock, R.A., and Gill, A.M., 2010, The initiation of fire spread in shrubland fuels recreated in the laboratory, International Journal of Wildland Fire, 19, 512-520.

Pollet, J., and Brown, A., 2007, Fuel moisture sampling guide, Bureau of Land Management, Utah State Office, Salt Lake City, Utah, USA.

Qi, Y., Dennison, P.E., Spencer, J., and Riaño, D., 2012, Monitoring live fuel moisture using soil moisture and remote sensing proxies, Fire Ecology, 8, 71-87.

Qi, Y., Dennison, P.E., Jolly, W.M., Kropp, R.C., and Brewer, S., 2014, Spectroscopic analysis of seasonal changes in live fuel moisture content and leaf dry mass, Remote Sensing of Environment, 150, 198-206.

Rautiainen, M., Mõttus, M., Yáñez-Rausell, L., Homolová, L., Malenovský, Z., and Schaepman, M.E., 2012, A note on upscaling coniferous needle spectra to shoot spectral albedo, Remote Sensing of Environment, 117, 469-474.

Reid, A.M., and Robertson, K.M., 2012, Energy content of common fuels in upland pine savannas of the south-eastern US and their application to fire behaviour modelling, International Journal of Wildland Fire, 21, 591-595.

Riaño, D., Vaughan, P., Chuvieco, E., Zarco-Tejada, P.J., and Ustin, S.L., 2005, Estimation of fuel moisture content by inversion of radiative transfer models to simulate equivalent water thickness and dry matter content: Analysis at leaf and canopy level, IEEE Transactions on Geoscience and Remote Sensing, 43, 819-826.

Richter, K., Atzberger, C., Hank, T.B., and Mauser, W., 2012, Derivation of biophysical variables from Earth observation data: Validation and statistical measures, Journal of Applied Remote Sensing, 6, 1-23.

Richards, J.H., and Caldwell, M.M., 1987, Hydraulic lift: Substantial nocturnal water transport between soil layers by Artemisia tridentata roots, Oecologia, 73, 486-489.

Roberts, D.A., Dennison, P.E., Peterson, S., Sweeney, S., and Rechel, J., 2006, Evaluation of Airborne Visible/Infrared Imaging Spectrometer (AVIRIS) and Moderate Resolution Imaging Spectrometer (MODIS) measures of live fuel moisture and fuel condition in a shrubland ecosystem in southern California, Journal of Geophysical Research, 111, G04S02, doi:10.1029/2005JG000113.

Rothermel, R.C., 1972, A mathematical model for predicting fire spread in wildland fuels, USDA Forest Service Research Paper INT-115, Intermountain Forest and Range Experiment Station, Ogden, UT.

Rouse, J.W., Haas, R.H., Schell, J.A., and Deering, D.W., 1973, Monitoring vegetation systems in the Great Plains with ERTS, Pages 309-317 in: S.C. Freden, E.P. Mercanti, M.A. Becker, editors, Third Earth Resources Technology Satellite-1 Symposium: Proceedings of a Symposium, NASA SP-351 I, NASA, December 10-14 1973, Washington, D.C., USA.

Running, S.W., 2006, Is global warming causing more, larger wildfires? Science, 313, 927-928.

Rutter, A.J., 1957, Studies in the growth of young of Pinus sylvestris L.: I. The annual cycle of assimilation and growth, Annals of Botany, 21, 399-426.

Schulze, E.-D., Beck, E., and Klaus, M.-H., 2005, Water relations of plants, Pages 277-311 in: E.-D. Schulze, E. Beck, and M.-H.Klaus, editors, Plant ecology, Springer, Berlin, Germany.

Scott, J.H., and Burgan, R.E., 2005, Standard fire behavior fuel models: A comprehensive set for use with Rothermel's surface fire spread model, Gen Tech Rep RMRS-GTR-153, Fort Collins, CO: US Department of Agriculture, Forest Service, Rocky Mountain Research Station, 72 p.

Sebastián-López, A., San-Miguel-Ayanz, J., and Burgan, R.E., 2002, Integration of

satellite sensor data, fuel type maps and meteorological observation for evaluation of forest fire risk at the pan-European scale, International Journal of Remote Sensing, 23, 2713-2719.

Serbin, S.P., Dillaway, D.N., Kruger, E.L., and Townsend, P.A., 2012, Leaf optical properties reflect variation in photosynthetic metabolism and its sensitivity to temperature, Journal of Experimental Botany, 63, 489-502.

Serrano, L., Ustin, S.L., Roberts, D.A., Gamon, J.A., and Peñuelas, J., 2000, Deriving water content of chaparral vegetation from AVIRIS data, Remote Sensing of Environment, 74, 570-581.

Sims, D.A., Rahman, A.F., Vermote, E.F., and Jiang, Z., 2011, Seasonal and inter-annual variation in view angle effects on MODIS vegetation indices at three forest sites, Remote Sensing of Environment, 115, 3112-3120.

Snyder, R., and W. Pruitt, 1992, Evapotranspiration data management in California, Pages 128-133 in: T. Engman, editor, Irrigation and drainage: Saving a threatened resource—In Search of solutions, American Society of Civil Engineers, New York, USA.

Stimson, H.C., Breshears, D.D., Ustin, S.L., and Kefauver, S.C., 2005, Spectral sensing of foliar water conditions in two co-occurring conifer species: Pinus edulis and Juniperus monosperma, Remote Sensing of Environment, 96, 108-118.

Stocks, B. J., Lawson, B.D., Alexander, M.E., Van Wagner, C.E., McAlpine, R.S., Lynham, T.J., and Dubé, D.E., 1989, The canadian forest fire danger rating system: An overview, The Forestry Chronicle, 65, 258-265.

Stow, D., Niphadkar, M., and Kaiser, J., 2005, MODIS-derived visible atmospherically resistant index for monitoring chaparral moisture content, International Journal of Remote Sensing, 26, 3867-3873.

Stow, D., Niphadkar, M., and Kaiser, J., 2006, Time series of chaparral live fuel moisture maps derived from MODIS satellite data, International Journal of Wildland Fire, 15, 347-360.

Stow, D, and Niphadkar, M., 2007, Stability, normalization and accuracy of MODIS-derived estimates of live fuel moisture for southern California chaparral, International Journal of Remote Sensing, 28, 5175-5182.

Stuckens, J., Dzikiti, S., Verstraeten, W.W., Verreynne, S., Swennen, R., and Coppin, P., 2011, Physiological interpretation of a hyperspectral time series in a citrus orchard, Agricultural and Forest Meteorology, 151, 1002-1015.

Tian, Q., Tong, Q., Pu, R., Guo, X., and Zhao, C., 2001, Spectroscopic determination of

wheat water status using1650-1850 nm spectral absorption features, International Journal of Remote Sensing, 22, 2329-2338.

Trombetti, M., Riaño, D., Rubio, M., Cheng, Y., and Ustin, S., 2008, Multi-temporal vegetation canopy water content retrieval and interpretation using artificial neural networks for the continental USA, Remote Sensing of Environment, 112, 203-215.

Ustin, S.L., Roberts, D.A., Pinzón, J., Jacquemoud, S., Gardner, M., Scheer, G., Castañeda, C.M., and Palacios-Orueta, A., 1998, Estimating canopy water content of chaparral shrubs using optical methods, Remote Sensing of Environment, 65, 280-291.

Van Der Werf, G.R., Randerson, J.T., Giglio, L., Collatz, G.J., Kasibhatla, P.S., and Arellano Jr, A.F., 2006, Interannual variability in global biomass burning emissions from 1997 to 2004, Atmospheric Chemistry and Physics, 6, 3423-3441.

Van Wagdendonk, J., Sydoriak, W., and Benedict, J., 1998, Heat content variation of Sierra Nevada conifers, International Journal of Wildland Fire, 8, 147-158.

Vermote, E.F., and Kotchenova, S., 2008, Atmospheric correction for the monitoring of land surfaces, Journal of Geophysical Research D: Atmospheres, 113, D23S90, doi:10.1029/2007JD009662.

Viegas, D.X., Pinõl, J., Viegas, M.T., and Ogaya, R., 2001, Estimating live fine fuels moisture content using meteorological-based indices, International Journal of Wildland Fire, 10, 223-240.

Wang, L., Qu, J.J., Hao, X., and Hunt Jr, E.R., 2011, Estimating dry matter content from spectral reflectance for green leaves of different species, International Journal of Remote Sensing, 32, 7097-7109.

Williamson, N.M., and Agee, J.K., 2002, Heat content variation of interior Pacific Northwest conifer foliage, International Journal of Wildland Fire, 11, 91-94.

Weise, D.R., Zhou, X., Sun, L., and Mahalingam, S., 2005, Fire spread in chaparral-'go or no-go?', International Journal of Wildland Fire, 14, 99-106.

Westerling, A.L., Hidalgo, H.G., Cayan, D.R., and Swetnam, T.W., 2006, Warming and earlier spring increase western US forest wildfire activity, Science, 313, 940-943.

Wold, S., Sjöström, M., and Eriksson, L., 2001, PLS-regression: A basic tool of chemometrics, Chemometrics and Intelligent Laboratory Systems, 58, 109-130.

Yebra, M., and Chuvieco, E., 2009, Linking ecological information and radiative transfer models to estimate fuel moisture content in the Mediterranean region of Spain: Solving the ill-posed inverse problem, Remote Sensing of Environment, 113,

2403-2411.

Yebra, M., Dennison, P.E., Chuvieco, E., Riaño, D., Zylstra, P., Hunt, E.R., Danson, F.M., Qi, Y., and Jurdao, S., 2013, A global review of remote sensing of live fuel moisture content for fire danger assessment: Moving towards operational products, Remote Sensing of Environment, 136, 455-468.

Yebra, M., Chuvieco, E., and Riano, D., 2008, Estimation of live fuel moisture content from MODIS images for fire risk assessment, Agricultural and Forest Meteorology, 148, 523-536.

Zarco-Tejada, P., 2003, Water content estimation in vegetation with MODIS reflectance data and model inversion methods, Remote Sensing of Environment, 85, 109-124.

Zhang, Y., Chen, J.M., Miller, J.R., and Noland, T.L., 2008, Retrieving chlorophyll content in conifer needles from hyperspectral measurements, Canadian Journal of Remote Sensing, 34, 296-310.

Zhao, K., Valle, D., Popescu, S., Zhang, X., and Mallick, B., 2013, Hyperspectral remote sensing of plant biochemistry using Bayesian model averaging with variable and band selection, Remote Sensing of Environment, 132, 102-119.